



1 Morphodynamics of the Mont Blanc glaciers and their recent 2 evolution

3 Fabrizio Troilo^{1,4}, Niccolò Dematteis³, Francesco Zucca⁴, Martin Funk², Daniele Giordan³.

4 ¹Fondazione Montagna sicura, Glaciers, snow and avalanche research area, Courmayeur, 11013, Italy.

5 ²ETH-VAW, Versuchsanstalt für Wasserbau, Hydrologie und Glaziologie, Zurich, CH-8092, Switzerland.

6 ³Research Institute for Geo-Hydrological Protection IRPI, Italian National Research Council, Turin, 10135, Italy.

7 ⁴University of Pavia, Department of Earth and Environmental Sciences, Pavia, 27100, Italy.

8 *Correspondence to: Niccolò Dematteis (niccolo.dematteis@irpi.cnr.it); Fabrizio Troilo (ftroilo@fondms.org).*

9 **Abstract.** The surface velocity of glaciers is a key parameter that provides fundamental information on glacier dynamics and
10 their adaptation to changes in climate; moreover, ice velocity measurements are a very important parameter for modelling
11 glacier physics and their evolution. While a few decades ago ice velocity would rely on point measurements performed in the
12 field, the processing of high temporal and spatial resolution information from satellites nowadays provides new insights and a
13 vast quantity of data, on a global scale, for the measurement of ice velocity. As of today, few studies have been performed in
14 Alpine regions, and rarely has the focus been on ice velocity evolution. In the present study, we analyse the average monthly
15 velocities on Alpine glaciers in the Mont Blanc massif. Seven years of Sentinel-2 optical satellite imagery have been processed
16 to obtain ice velocity data. The main objectives of the study are: (i) to characterise the variability of the velocity fields of such
17 glaciers, referring both to their temporal (seasonal and interannual) and spatial variations; (ii) to find relationships between the
18 morphology of glaciers and their kinematics. We measured the monthly velocities of thirty glaciers varying from 18.0 m yr⁻¹
19 to 436.3 m yr⁻¹, highlighting a breakpoint in the trends in 2020. This led to the identification of 13 glaciers showing variation
20 of more than 20.0 m yr⁻² between 2020 and 2022 compared to the previous years. We identified five clusters of morpho-
21 dynamic characteristics, thus describing five different glacier type classes.

22 1 Introduction

23 Glacier flow has been one of the early drivers of glaciological interest and research since it was first studied. Its understanding
24 and modelling evolved via the observations and findings of Somigliana in the early 1900s, Glen's laboratory experiments
25 (Glen, 1952), followed by the interpretations of Nye (Nye, 1952) during the 1950s, to cite just a few, and have explained that
26 the two main mechanisms of glacier flow rely on ice deformation and basal sliding. However, the motion of Alpine glaciers is
27 largely related to basal sliding (Willis, 1995). Continuous monitoring of sliding velocities is extremely difficult and rarely
28 achieved (Vincent and Moreau, 2016), but also the continuous monitoring of surface velocities of Alpine glaciers is complex
29 on specific study sites, and very rarely has it been performed on a spatially distributed scale.

30 The flow of glaciers generally depends on a variety of physical parameters: ice thickness, which is the main driver of ice flow
31 (Jiskoot 2011), and is related indirectly to the glacier trend in mass balance as it determines an evolution towards increase or
32 decrease in glacier thickness; the glacier surface slope which is the other fundamental driver of ice flow; other parameters that
33 influence ice flow are: ice properties (temperature, density), bedrock conditions (hard, soft, frozen or thawed ice-bed contact),
34 topography, the glacier's terminal area type (land, sea, ice shelf), but also air temperature and precipitation and their seasonality
35 that influences subglacial hydrology (Jiskoot, 2011; Humbert et al., 2005; Cuffey and Paterson, 2010; Benn and Evans, 2014;
36 Bindshadler, 1983).



37 The analysis of glacier surface displacements is often measured as a proxy of ice flow and has a wide array of applications: it
38 is a powerful climate change indicator (Beniston et al., 2018). It is also an important input data for global ice thickness models
39 (Millan et al., 2022; Samsonov et al., 2021) which estimate global freshwater resources and global mass balance models that
40 can also approximate sea-level rise contribution by glaciers (Zekollari et al., 2019). In the field of glacial hazards, it is used as
41 a proxy for the detection of glacier surges (Kamb, 1987; Käab et al., 2021), and accelerations that can result in glacier-related
42 hazards (Pralong and Funk, 2006; Giordan et al., 2020). Measurements of the surface velocity of glaciers can be achieved by
43 terrestrial techniques (Dematteis et al., 2021) such as topographic measurements of stakes or fixed points on the glacier
44 (Stocker-Waldhuber et al., 2019), GNSS repeated or continuous surveys (Einarsson et al., 2016), digital image correlation of
45 oblique photographs (Evans, 2000; Ahn and Box, 2010) and terrestrial radar interferometry (Luzi et al., 2007; Allstadt et al.,
46 2015).

47 Considering remote sensing solutions, glacier surface velocities can be measured by a variety of aerial and space borne sensors.
48 In recent decades, public access to satellite optical and radar data (especially from Sentinel and Landsat constellation satellites),
49 as well as the commercial availability of very high resolution (30 cm to 1 m ground resolution) optical imagery (Deilami and
50 Hashim, 2011) and radar data (Rankl et al., 2014), have given great input to glaciological research. In particular, Sentinel-2
51 optical imagery is widely used in glaciological studies and has been tested in literature on various environments (Paul et al.,
52 2016; Millan et al., 2019). Nowadays, the automated processing of ice velocity maps with global coverage from satellite
53 imagery is freely available online from web-based platforms such as the Golive datasets (Fahnestock et al., 2016), the ITS
54 Live dataportal (<https://its-live.jpl.nasa.gov/>) or the FAU-Glacier portal (RETREAT, 2021 Ice surface velocities derived from
55 Sentinel-1, Version 1; <http://retreat.geographie.uni-erlangen.de/search>). The availability of such datasets is very relevant
56 globally, but its application to Alpine glaciers is limited due to its relatively coarse spatial resolution - e.g., 300x300 m
57 (Golive), 120x120 m (ITS live) - which can provide data on just few of the largest Alpine glaciers. The adopted resolution is
58 a trade-off between computational effort and best resolution of the output that must cope with the global availability of the
59 analysis. Limiting the processing of images at a regional scale decreases the computational effort compared to global products
60 and makes it easier to obtain higher resolution velocity maps that allows Alpine glaciers to be investigated (Berthier et al.,
61 2005), even though very small glaciers (i.e., width <250 m) are still difficult to analyse (Millan et al., 2019).

62 Recent studies using different techniques have measured spatio-temporal variations of ice velocity on large valley glaciers in
63 an Alpine environment (Argentièrre Glacier) (Vincent and Moreau, 2016) (Miage Glacier) (Fyffe, 2012) as well as on steep
64 glacier snouts (Planpincieux Glacier) (Giordan et al., 2020) but a spatially distributed analysis, at a regional scale, of the
65 variations of velocities over glaciers with different morphological characteristics is, as of today, still lacking in the Alpine
66 environment.

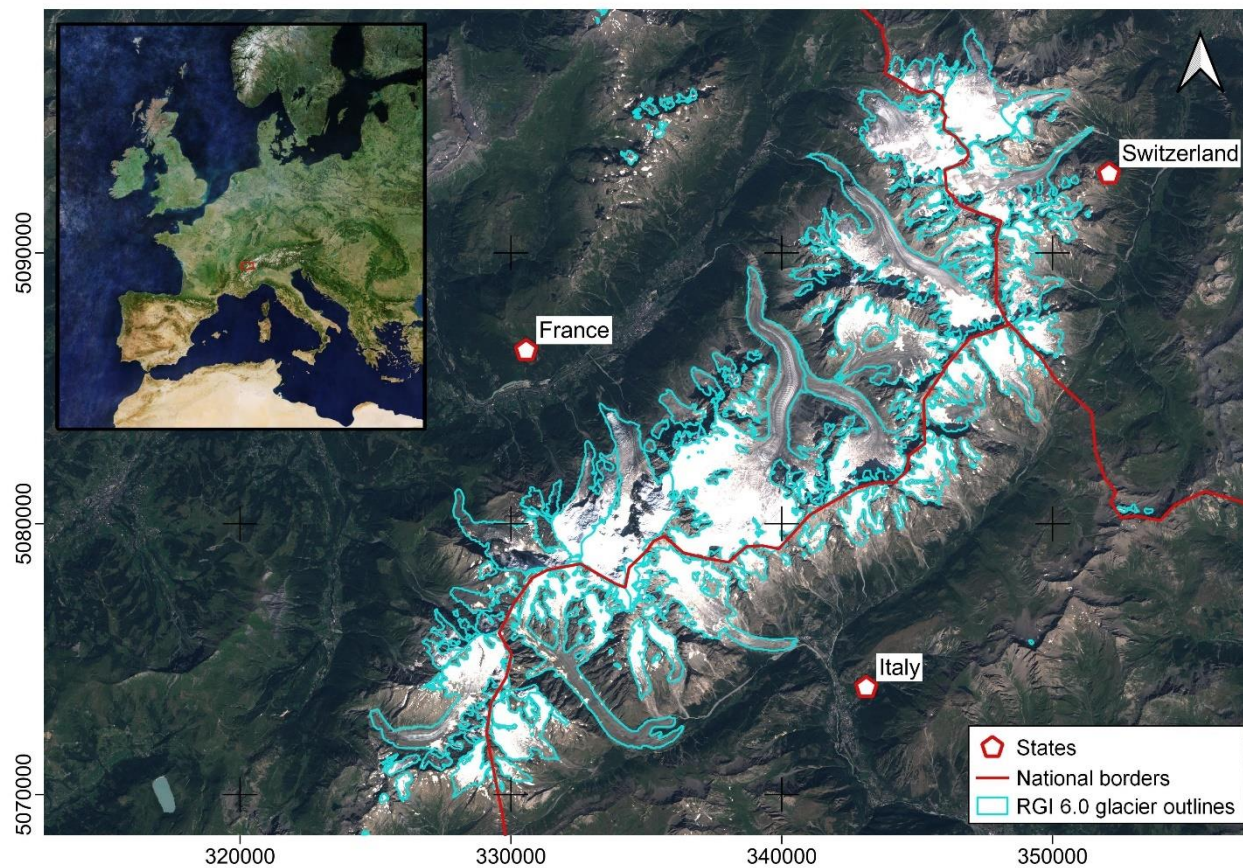
67 The main purposes of this study are the production of seven year-long velocity time series of surface velocity of thirty glaciers
68 at a massif scale, as well as an integrated analysis of morphological and kinematic features of such glaciers. The identification
69 of possible trends in the velocity time series, and a classification based on kinematic and morphological features, are major
70 objectives of the present study. We analysed seven years of Sentinel-2 optical imagery to retrieve monthly velocity data on
71 thirty glaciers in the Mont Blanc massif. We describe different patterns and behaviours of surface; subsequently, a classification
72 based on velocity and morphometric features is proposed.

73 **2 Area of study**

74 The study area is the Mont Blanc massif. It is located in the western part of the European Alps bordering France, Italy and
75 Switzerland (Figure 1) and culminating at 4809 m with the Mont Blanc summit; the highest peak in Central Europe. Many



76 other peaks in the Mont Blanc massif reach well above 4000 m and the entire area is very highly frequented with famous
77 tourist resorts such as Courmayeur and Chamonix attracting thousands of tourists every year.



78
79 **Figure 1. Study area of the Mont Blanc massif. Background: true colour image (cloud-free Europe mosaic in upper left panel),**
80 **courtesy of the Copernicus Open Access Hub (<https://scihub.copernicus.eu>, last access: 10 September 2023).**

81
82 The total surface of glaciers in the Mont Blanc massif is equal to 169 km² and totals 116 glaciers, according to the Randolph
83 glacier inventory (RGI) 6.0 data which refers to 2003 (Pfeffer et al., 2014; Arendt et al., 2017). Seventy-six glaciers are very
84 small, covering an area of less than 0.1 km², twenty-eight glaciers fall in the range between 1 km² and 5 km², and twelve
85 glaciers have surface areas of more than 5 km².

86 The geological setting and the geomorphology of the Mont Blanc massif forms a high mountain range with its main ridge line
87 oriented in a south-west/north-east direction along the French-Italian border. The valley floors flanking the massif have low
88 altitudes - in the range of 1000-1500 m - resulting in steep slopes originating from the highest peaks with large vertical
89 altitudinal differences. The meteo-climatic local conditions on the massif are of a continental type, but orographic effects on
90 the predominant incoming weather fronts mean larger amounts of local precipitation compared to nearby regions (Gottardi et
91 al., 2012).

92 The Argentière Glacier is the only glacier with regular mass balance measurements included in the WGMS 'Reference
93 Glaciers' dataset in the Mont Blanc massif (Zemp et al., 2009). The Argentière Glacier has shown a general negative mass



94 balance trend since the early 1990s, in line with mass balances of other Alpine glaciers and glaciers from other mountain
95 ranges across the globe. Geodetic mass balance measurements of the Thoula Glacier, a small glacier on the border between
96 France and Italy at altitudes between 2900 and 3300m, represent well the local meteo-climatic conditions that result in slightly
97 less negative mass balance trends compared to other glaciers in the Alps (Zemp et al., 2021; Zemp et al., 2020; Mondardini et
98 al., 2021).

99 A more spatially distributed analysis of mass balances in the Mont Blanc region has also been outlined in the literature by
100 means of geodetic mass balances of the whole Mont Blanc massif using stereo satellite imagery from the Pléiades and Spot
101 satellite constellations (Berthier et al., 2014; Beraud et al., 2023). The trend outlined by Berthier (2014) at the massif scale,
102 reflects data trends comparable to the glaciological mass balances of WGMG reference glaciers in the Alps. Locally, glaciers
103 at a very low altitude show large ice volume losses and subsequent substantial glacier front retreats (Paul et al., 2020), while
104 glaciers at higher altitudes suffer less acute volume loss and shrinkage. Large differences in the glacier frontal position,
105 especially for the lower altitude terminating glaciers, can be well assessed by the difference of the terminus position in recent
106 satellite imagery compared to the position outlined on the Randolph Glacier Inventory (RGI).

107 **3 Materials**

108 In this paper, we analysed the Copernicus - ESA Sentinel-2 optical satellite imagery dataset available for the study area. In
109 addition to the above-mentioned dataset, we used Airbus Pleiades Stereo derived digital elevation models (DEMs) for the
110 morphometric analysis of glaciers, and publicly available modelled ice thickness data from Millan et al. (Millan et al., 2022).

111 **3.1 Sentinel-2 optical satellite imagery**

112 The Sentinel-2 mission is composed of twin satellites - Sentinel-2A and Sentinel-2B - orbiting on sun-synchronous orbits at
113 an altitude of 786 km. Free availability of thirteen multispectral bands (443 nm-2190 nm central wavelengths) with ground
114 resolutions ranging between 10 m and 60 m, and a revisit time as low as three days for some areas (five days for most areas),
115 as well as global coverage, make this product a very important resource for glaciological studies. In particular, Sentinel-2 near
116 infrared band B08 processing level L1C is used for the application of feature tracking on glacial surfaces, as suggested by
117 previous studies (Kääb et al., 2016). Based on different publications (Kääb et al., 2016; Millan et al., 2019), the geometric
118 error of Sentinel-2 can show up to 1.5 pixel offsets in the horizontal plane. Therefore, an image co-registration process is
119 normally needed for multitemporal analyses.

120 In the present study, a set of 108 images between 5 February 2016 and 10 November 2022, covering the whole study area, was
121 adopted (GRANULE T32TLR, relative orbit 108). Such images, named ‘tiles’, are ~110x110 km² ortho-images in
122 UTM/WGS84 projection.

123 **3.2 Morphometric analysis data**

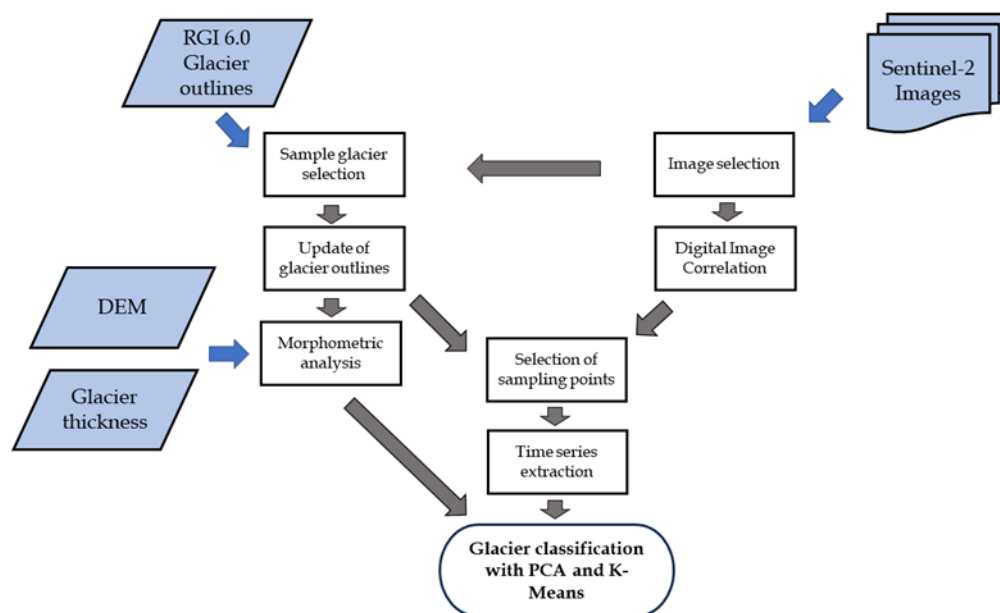
124 Morphometric analysis of sample glaciers was performed using altitudinal data from a 1m resolution DEM obtained by the
125 processing of Pleiades stereo pairs from August 2018 (Berthier et al., 2014). Mean glacier thicknesses were extrapolated from
126 globally modelled ice thickness data published by Millan et al. (Millan et al., 2022).



127 4 Methods

128 We used digital image correlation to produce monthly-averaged and multi-year averaged velocity maps to investigate
129 variations of glacier surface velocity in time and in space over the selected glaciers. We can hereby summarize the workflow
130 that was used (Figure 2):

131



132

133 **Figure 2. Workflow of the present study. The input datasets are evidenced in light blue while the processing steps are indicated in**
134 **grey.**

135

136 The input data are a DEM of the area of study, the RGI glacier outlines, the modelled glacier thickness and the stack of
137 Sentinel-2 images in the reference period. The input DEM is used to obtain morphometric parameters of the glacier while the
138 RGI glacier outlines are used, together with the selected satellite imagery, to choose suitable glaciers for surface glacier
139 velocity analysis. After the glacier selection, we updated the RGI glacier outlines. Selected imagery is processed with digital
140 image correlation to obtain glacier velocities. The glacier surface velocity maps are then used, together with the updated glacier
141 outlines, to identify suitable areas and sampling points to extract velocity time series. Time series are analysed to identify
142 general trends, seasonal patterns or particular kinematic behaviours. Finally, the velocity dataset and the morphometric
143 parameters are analysed with a principal component analysis (PCA); subsequently, the principal components (PCs) are
144 clustered using a K-means analysis to determine different classes of glacier based on their morpho-dynamic features.

145 4.1 Sentinel-2 image selection

146 To select the images, we considered two elements: (i) to maximize the geometric and geo-referencing precision, we adopted
147 images acquired from the same orbit; (ii) to reduce the impact of clouds, we carried out a visual check of all images with a
148 cloud cover percentage lower than 90% (as detected by the Copernicus cloud cover estimation algorithm) on the whole tile.
149 We adopted this manual selection to maximize the number of available images; in the case of the Mont Blanc massif (like in



150 most mountainous areas worldwide), the local distribution of clouds can be extremely variable; in many cases, this can
151 contribute to a considerable cloud percentage, even though high altitude areas may still be cloud-free.

152 **4.2 Glacier selection**

153 In the Mont Blanc massif, the presence of high-altitude accumulation areas, together with steep slopes, results in a significant
154 number of very active glaciers with high average velocities in a relatively small region. In the present study, we selected a set
155 of glaciers and investigated their surface velocity.

156 To minimize the presence of noisy and unreliable velocity data, we performed a selection of glaciers from the RGI 6.0 dataset.
157 In particular, we did not include in our study:

158 A) glaciers with area $< 0.1 \text{ km}^2$, as those glaciers would be too small for the reliable extraction of velocity maps with 10 m
159 resolution optical satellite imagery (Millan et al., 2019).

160 B) glaciers showing strong variations of cast shadow.

161 C) glaciers that lack surface features to be tracked (e.g., ice caps).

162 Selection of point B) was made by creating a stack of images acquired between October and March, when cast shadows appear
163 on satellite imagery, especially on north facing slopes. Subsequently, we manually individuated glaciers that are subject to
164 large variations of shadow on their surface. We used the scene classification map (SCL) class 11 (cast shadows), available in
165 processing level L2A of the Sentinel-2 images. However, since shadows on glaciers may often be misclassified in wintry
166 conditions, we conducted a manual check to correct potential errors.

167 Selection of point C) is made manually by selecting glaciers that show very even surfaces on Sentinel-2 images. This is
168 normally noted in ice caps at higher altitudes.

169 **4.3 Glaciers' outline delineation**

170 To analyse glacier areas and have an up-to-date mapping of glacier areas, we updated RGI 6.0 glacier outlines in order to fit
171 with the glacier extensions that can be observed and manually outlined from Sentinel-2 imagery. We selected a cloud-free
172 scene acquired on 28 August 2018 that represents well the conditions of the glaciers in the study period; True Color Image
173 was used for this purpose. In some cases, a morphological indication that some parts of the glaciers could be considered
174 independently from others in a division of kinematic domains was individuated (Paul et al., 2022; Zemp et al., 2021). As the
175 kinematic analysis confirmed distinct behaviours of some glacier parts, those glaciers were mapped accordingly. The main
176 examples of this are the tributary glaciers of the larger Miage Glacier complex, which all have distinct kinematic behaviour,
177 well differentiated from the slow-moving, debris-covered main central valley tongue. Another example is present at Talèfre
178 Glacier, where, over the past twenty years, the western part of the glacier has become totally independent from the eastern
179 section so it made sense to consider it as a single glacier as of the RGI mapping of 2003. However, it should be considered
180 independently in this study and consequently mapped.

181 **4.4 Glaciers' morphometric analysis**

182 The morphology that characterizes the glaciers selected in this study was analysed with the individuation of a series of key
183 morphometric parameters:

184 1) the glacier planimetric surface (*Area*),

185 2) the glacier mean slope (*Slope*),

186 3) the glacier mean thickness (*Thickness*), obtained using the free dataset of Millan et al (Millan et al., 2022).



187 4) the glacier elongation evaluated as the ratio between glacier length and area (Shape).
188 5) the accumulation area ratio (AAR). The AAR is a common parameter used in glaciological studies to define the ratio between
189 a snow-covered accumulation area and a bare ice ablation area of a specific glacier, at the end of the summer season. This
190 gives an indication of the tendency of a glacier to tend towards stable or mass gain conditions or towards a mass loss condition
191 (Cuffey and Paterson, 2010). AAR was obtained by mapping the snow accumulation areas on Sentinel-2 satellite images for
192 every year between 2016 and 2022 at the end of the melting season. Subsequently, we calculated the average AAR for the
193 study period.

194 **4.5 Glaciers' surface velocity mapping**

195 Digital image correlation is a common technique used to measure surface displacements using proximal (Evans, 2000; Ahn
196 and Box, 2010; Schwalbe and Maas, 2017) and remotely sensed imagery (Scambos et al., 1992; Heid and Kääb, 2012b; Marsy
197 et al., 2021; Dematteis and Giordan, 2021). The processing chain performed in the present study uses the open-source Glacier
198 Image Velocimetry (GIV) toolbox (Van Wyk De Vries and Wickert, 2021). GIV uses frequency-based correlation, can process
199 large datasets efficiently way and has been shown to perform well on glacier surface velocity measurements at different test
200 sites (Van Wyk De Vries and Wickert, 2021). Co-registration of images is implemented in the GIV process chain using a stable
201 area where potential shifts are estimated. To measure glacier surface velocities, we adopted the 'multi-pass' option which
202 updates displacement estimates over multiple iterations, refining initial coarse chip size displacement calculations using
203 progressively smaller chip sizes. The initial chip size is automatically defined by GIV and cannot be smaller than 32x32 px.
204 Velocities higher than 1500 m yr⁻¹ were considered as unrealistic and discarded. Grid spacing of the nodes in the displacement
205 maps was set to 40 m. To produce the time series, given a specific image, we processed the first and second subsequent images
206 (GIV order 2 time-oversampling). Then, the velocities of image pairs were averaged on a monthly basis. A temporal and spatial
207 smoothing function was implemented in the processing algorithm and was used in the processing of data in this study.

208 **4.6 Selection of sampling points**

209 To analyse the time series that are representative of velocity variations of the selected glaciers, sampling points were identified
210 on the velocity maps. The selection of sampling points for the time series extraction was carried out manually on the glacier
211 surface, focusing on areas where velocity maps show high spatial coherence (Altena et al., 2019).
212 In some cases, the sampling points are not evenly distributed; when this occurred, the sampling points were located in areas
213 that highlight velocity peaks (areas that show larger displacements than the surrounding areas) and high spatial coherence and
214 that show no data voids (areas with unsuccessful image pair matching results in missing values). For each of the selected
215 glaciers we analysed representative sectors: we extracted a variable number of sampling points ranging from 10 to 30 according
216 to the glacier size and morphology.

217 **4.7 Velocity time series extraction**

218 Once we defined the sampling points for every selected glacier, we extracted the monthly time series of velocity by averaging
219 the values of all the sampling points. Outliers' removal in the time series was performed via a manual check of the data.
220 We derived the velocity trend using an iteratively re-weighted least squares linear fit. To evaluate the significance of the fit
221 coefficient, we consider the ratio between the coefficients and their standard errors; this equates to the *t*-statistics to test the
222 null hypothesis that the corresponding coefficient is zero against the alternative that it is different from zero. That is, the lower
223 the *t*-statics is, the lower the statistical significance of the obtained coefficient is.



224 Subsequently, we analysed a set of specific parameters:

225 A) GlobalAvg: the median global velocity during the whole considered period.

226 B) GlobalVar: the velocity min/max range (excluding the outliers $v < Q_1 - 1.5(Q_3 - Q_1)$ or $v > Q_3 + 1.5(Q_3 - Q_1)$, where
227 Q_1 are the first and third quartiles of monthly velocity)

228 C) SeasonalVar: the mean difference between the average velocities during the ablation season (i.e., from July to September)
229 and the during the accumulation season (i.e., from December to April). The reference periods were chosen according to periods
230 of acceleration and slow down measured at Planpincieux Glacier by Giordan et. Al (2020).

231 D) MaxAnom: the ratio between the maximum monthly velocity and GlobalAvg.

232 4.8 Glacier classification

233 We investigated the presence of distinct classes of glacier based on their morphodynamics using PCA and K-means clustering.
234 PCA is a multivariate analysis technique that allows a reduction in the dimensionality of a given dataset, increasing
235 interpretability but minimising information loss. This is achieved by creating new, uncorrelated variables that successively
236 maximise the variance of the dataset (Jolliffe and Cadima, 2016). We applied PCA to the morphometric and kinematic features
237 listed in Sections 4.3 and 4.7, respectively. Since PCA performs better with data of similar magnitude, we normalized the data
238 by subtracting the mean and dividing it by the standard deviation (Figure S2).

239 The K-means clustering method is an unsupervised machine-learning technique used to identify clusters of data objects in a
240 dataset. It is largely used in the analysis of remote-sensed data and earth observation data (Paradis, 2022). We applied the K-
241 means algorithm to the two principal components (PCs), considering five classes.

242 5 Results

243 We obtained detailed kinematic data from thirty glaciers in the Mont Blanc massif. Different kinematic behaviours were
244 analysed and compared to the morphometrics of the glaciers studied. Some particular seasonal kinematics were highlighted,
245 and particularities in the average velocity trends observed. A brief description of all the glaciers we analysed is found in
246 Appendix 1 to describe the location and geomorphological setting of the glaciers as well as highlight when a single glacier
247 complex from the RGI inventory was divided into independent glacial bodies because of very distinct kinematic behaviour.
248 We therefore detail all the results obtained in the present study in the following sections.

249 5.1 Sentinel-2 image selection

250 To select the Sentinel-2 images for glacier analysis, we discarded tiles with cloud cover, as detected by the Copernicus scene
251 classification, of higher than 90% due to the low possibility of having cloud-free conditions in the study area. From 1 January
252 2016 to 31 December 2022, a total of 295 images with a cloud cover percentage lower than 90% was analysed. Of these
253 images, 135 derive from Sentinel S2B and 160 from Sentinel S2A. From this dataset, we extracted a subset of 105 images that
254 are cloud free on the selected glacier areas via the visual inspection of the individual images. The number of suitable images
255 that are available per year varies from 10 to 21 with a yearly mean of 15 images in the following distribution: 2016: 10; 2017:
256 18; 2018: 10; 2019: 14; 2020: 11; 2021: 21; 2022: 21.

257 Year 2016, and partially 2017, is influenced by the lack of Sentinel 2B images. In fact, while Sentinel 2A was launched on 23
258 June 2015, Sentinel 2B was launched on 7 March 2017; image availability variations on the following years is influenced by

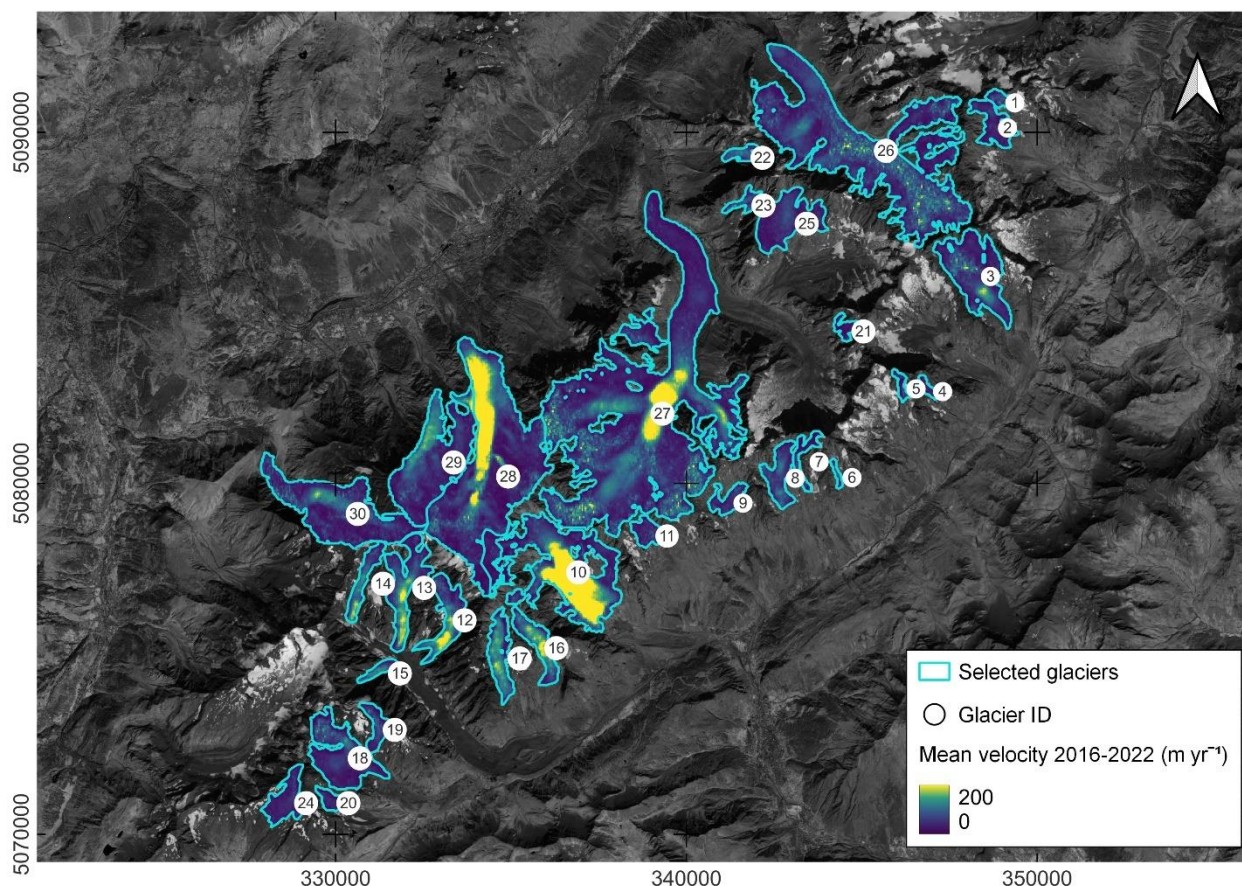


259 cloud cover at the time of scene acquisition. We chose to start the analysis from 2016 because it was the first full year of
260 acquisition from the satellite.

261 5.2 Glacier velocity mapping and selection, outline delineation and morphometric analysis

262 The glacier selection process identified thirty glaciers with a total glacierised surface of 85.8 km². Compared to the total
263 glacierised surface of the massif from RGI 6.0, this represents the covering of 50.8% of the total 169 km² and 25.9% in terms
264 of number of glaciers; this rises to 39.5% if we consider the subset of seventy-six glaciers having a glacierised surface of more
265 than 0.1 km². The selected glaciers are highlighted in Figure 3 and listed in Table 1, while a short description of each glacier
266 is provided in the Supplementary. Two of the selected glaciers are located in Switzerland, ten are located in France and eighteen
267 in Italy. This distribution is mainly due to a small portion of the massif being located in Switzerland and the presence of more
268 fragmented glacierised bodies on the Italian side. Of the thirty glaciers, seven have been mapped as sub-areas in comparison
269 to RGI individual glacier bodies.

270 In Figure 3 we present a velocity map with a resolution of 40 m (an masked over free-ice terrain in provided in Figure S1).
271 This was obtained by averaging all the single monthly averaged velocity maps in the study period (2016-2022).



272
273 **Figure 3. Surface glacier velocity map averaged in the 2016-2022 period. Selected glaciers for specific analyses are outlined in cyan.**
274 **Background: Sentinel-2 image (B08 band), courtesy of the Copernicus Open Access Hub (<https://scihub.copernicus.eu>, last access:**
275 **10 September 2023).**



276

277 **Table 1. Name and identification codes of glaciers selected for analysis in the present study. Codes from RGI and IDs used for**
 278 **simplicity in this study together with main morphometric parameters analysed in this study.**

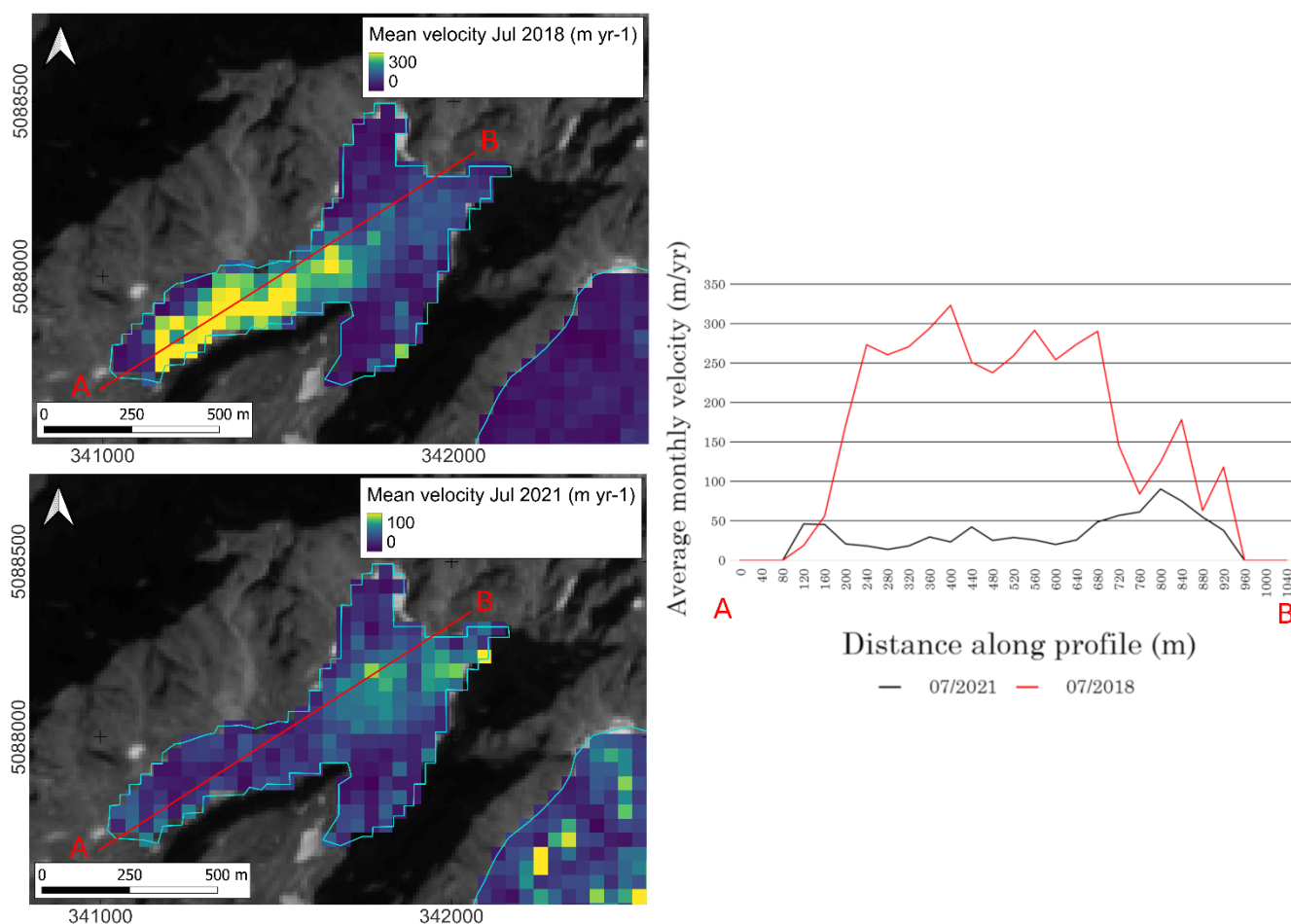
Glacier name	ID	RGI 6.0 ID	Area (km ²)	Length (m)	Min alt (m asl)	Max alt (m asl)	Avg slope (°)	Mean ice thickness (m)	Elongation ratio
A Neuve N	1	RGI60-11.02859	0.269	793	3084	3454	25.0	23.60	2.95
A Neuve Central	2	RGI60-11.02864	0.889	1800	2664	3554	26.3	26.29	2.02
Pre de Bard	3	RGI60-11.02916	3.011	3300	2360	3641	21.2	62.95	1.10
Greuvettaz E	4	RGI60-11.02978	0.196	985	2948	3582	32.8	11.88	5.03
Greuvettaz W	5	RGI60-11.02981	0.169	837	2704	3291	35.0	11.67	4.95
Planpincieux	6	RGI60-11.02991	1.013	2050	2627	3650	26.5	44.52	2.02
Grandes Jorasses	7	RGI60-11.02991	0.482	2110	2701	4206	35.5	15.27	4.38
Pra Sec	8	RGI60-11.02996	0.119	873	2536	3190	36.8	9.12	7.34
Rochefort	9	RGI60-11.03000	0.558	995	2720	3301	30.3	24.48	1.78
Brenva	10	RGI60-11.03001	6.579	4492	2374	4766	28.0	80.30	0.68
Thoula	11	RGI60-11.03002	0.58	1075	2880	3416	26.5	25.26	1.85
Mont Blanc	12	RGI60-11.03005	0.764	2486	2776	3773	21.9	46.85	3.25
Dome	13	RGI60-11.03005	1.973	3553	2453	4121	25.1	51.03	1.80
Bionassay (IT)	14	RGI60-11.03005	1.354	2926	2467	3816	24.8	52.69	2.16
Aiguille de Tre la tete N	15	RGI60-11.03005	0.312	1355	2408	3010	24.0	78.47	4.34
Freny	16	RGI60-11.03013	1.017	2623	2420	3698	26.0	60.74	2.58
Brouillard	17	RGI60-11.03014	1.166	2733	2499	3972	28.3	52.28	2.34
Lex Blanche	18	RGI60-11.03020	2.64	2450	2467	3757	27.8	41.40	0.93
Petit Mont Blanc	19	RGI60-11.03020	0.556	1767	2863	3580	22.1	26.31	3.18
Estelette	20	RGI60-11.03022	0.291	950	2716	3214	27.7	23.74	3.26
Pierre Joseph	21	RGI60-11.03258	0.275	710	2920	3409	34.6	14.77	2.58
Nant Blanc	22	RGI60-11.03263	0.363	1150	2600	3351	33.1	33.23	3.17
Charpoua	23	RGI60-11.03284	0.322	1211	2650	3479	34.4	25.41	3.76
Des Glaciers	24	RGI60-11.03339	1.091	2050	2735	3815	27.8	31.19	1.88
Talèfre N	25	RGI60-11.03466	2.037	1950	2700	3550	23.6	39.24	0.96
Argentière	26	RGI60-11.03638	13.109	7850	2178	3847	12.0	88.90	0.60
Mer de Glace	27	RGI60-11.03643	23.556	12090	1774	4025	10.5	103.75	0.51
Bossons	28	RGI60-11.03646	11.319	6795	1691	4776	24.4	59.66	0.60
Taconnaz	29	RGI60-11.03647	4.994	4291	2043	4286	27.6	40.15	0.86
Bionassay (FR)	30	RGI60-11.03648	4.774	5241	1835	4287	25.1	39.83	1.10

279 5.3 Spatial distribution of velocity patterns

280 Most glaciers can show seasonal velocity changes, as well as less markedly interannual velocity variations. Despite those
 281 variations, they maintain a constant spatial distribution of the velocity patterns on the velocity maps. To detect possible
 282 variations of the spatial distribution of velocities, we analysed single monthly maps on the selected glaciers for both winter



283 and summer months. This analysis led to the individuation of one glacier in particular - Charpoua Glacier (ID:23) - on which
284 the spatial distribution of velocities can be significantly different (Figure 4). In fact, years that present surge-like behaviour
285 show higher velocities towards the frontal part of the glacier while years that do not show surge-like activity show higher
286 velocities in the higher part of the glacier (Figure 4).



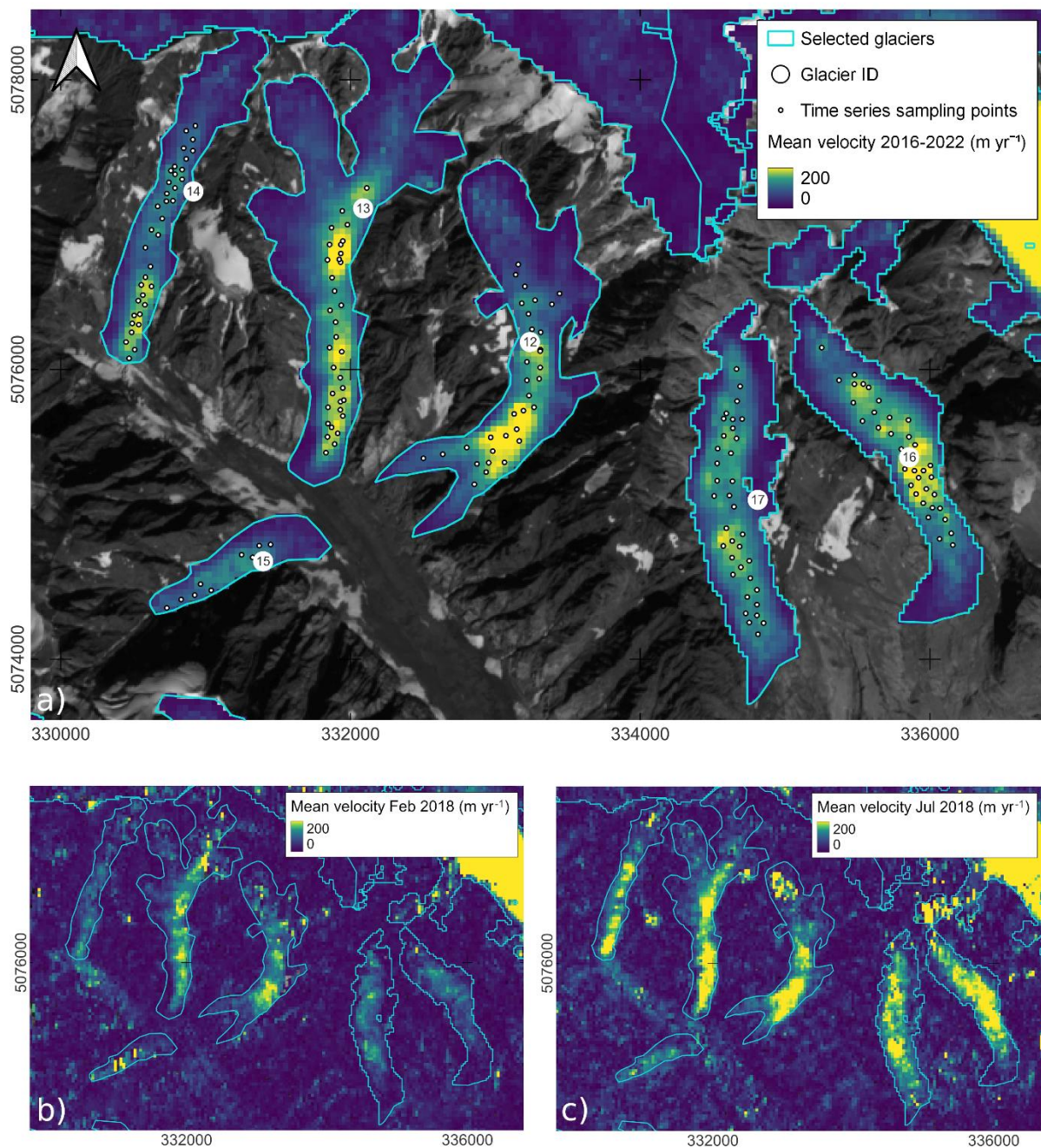
287
288 **Figure 4.** Charpoua Glacier (ID: 23) monthly surface velocity maps showing spatial variation of the velocity patterns in between
289 July 2018 (upper left) and July 2021 (lower left); note the different colour scales to highlight spatial distribution of values. The right
290 panel shows the average monthly velocity profile along a longitudinal west-east profile (in red on the maps, the profile start at A is
291 altitudinally lower) with July 2018 values in red and July 2021 values in black. Sentinel-2 imagery base map (B08 band), courtesy
292 of the Copernicus Open Access Hub (<https://scihub.copernicus.eu>, last access: 10 September 2023)

293 5.4 Selection of sampling points

294 Within every selected glacier, we manually identified ten to thirty points, depending on the glacier size, to extract velocity
295 time series. The points were distributed on the glacier surface evenly when possible, or avoiding areas with low spatial
296 coherence in the velocity maps which could be linked to local areas that suffered unsuccessful image matching. The presence
297 of cloud or snow on the glacier surface made it impossible to extract reliable data in the following periods: i) January 2017 ii)
298 December 2020, January and February 2021. However, the gaps represent only four months of no data out of the seven years



299 considered in the study (i.e., <5%). In Figure 5, we present an example of the obtained velocity map and the distribution of
300 sampling points over several chosen glaciers.



301
302 **Figure 5. a)** Details of glacier surface velocity map averaged in the 2016-2022 period and sampling points of selected sample glaciers.
303 **From left to right:** Bionassay (IT) Glacier – ID 14; Tre la Tete N Glacier – ID 15; Dome Glacier – ID 13; Mont Blanc Glacier – ID
304 12, Brouillard Glacier - ID 17; Freney Glacier – ID 16. Note that on smaller glaciers there is a limited number of sampling points
305 because of their limited area; on medium glaciers there is a distribution of points over all areas that show velocity maps with high



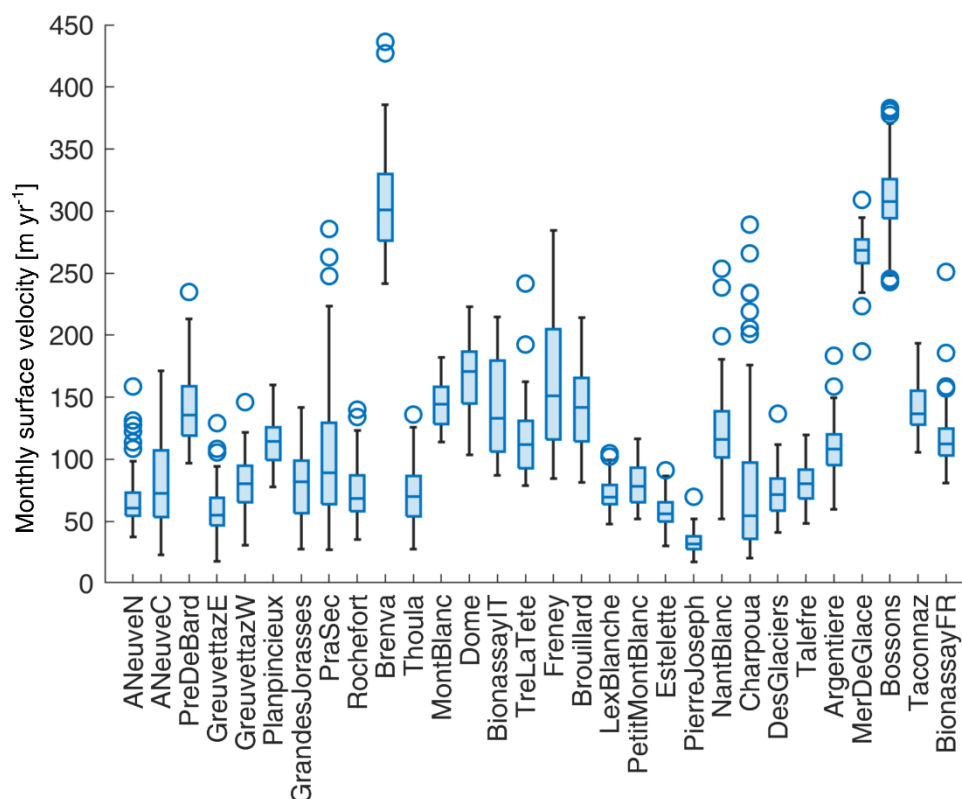
306 spatial coherence. Sentinel-2 imagery base map (B08 band), courtesy of the Copernicus Open Access Hub
307 (<https://scihub.copernicus.eu>, last access: 10 September 2023). Lower left (b) and right panels (c) show single average monthly
308 velocity maps of February and July 2018 respectively.

309 5.5 Velocity time series extraction

310 On the thirty glacial bodies we investigated in this study, the monthly velocity values range from 30-40 m yr⁻¹, typically
311 reached during winter months, to 350 and 400 m yr⁻¹, typically reached in summer/late summer. Such high velocity values are
312 attained by just a few of the largest glaciers in the dataset. In particular, monthly extreme values vary from 18.0 m yr⁻¹ reached
313 on January 2020 by the Greuvettaz E Glacier, to 436.3 m yr⁻¹ reached by the Brenva Glacier in July 2016.

314 Figure 6 presents the distributions of the monthly velocity of the considered glaciers. The mean surface velocities averaged
315 over the whole period range from 33.7 m yr⁻¹ at the Pierre-Joseph Glacier to 309.7 m yr⁻¹ at the Bossons Glacier. The standard
316 deviation of the velocity time series of single glaciers varies from 8.9 m yr⁻¹ at Pierre Joseph Glacier to 57.7 and 62.6 m yr⁻¹ at
317 the Pra Sec and Charpoua glaciers, respectively.

318



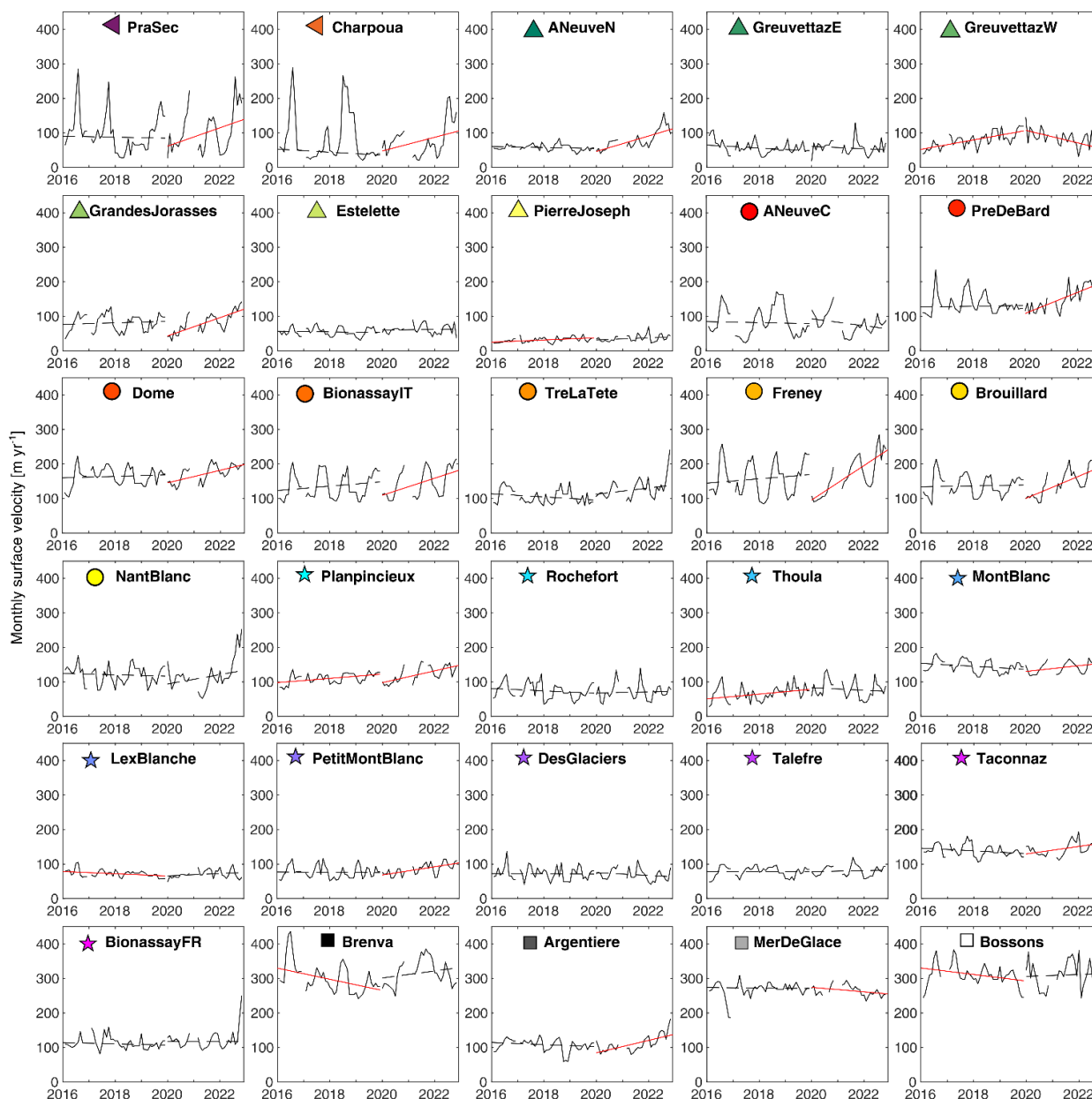
319

320 **Figure 6. Boxplot of the glaciers monthly averaged surface velocity.**

321 Velocity time series of the 30 analysed glaciers are represented in Figure 7. Glaciers such as the Freney, Brouillard, Dome,
322 Mont Blanc and Bionassay (IT) show large seasonal variability while others, such as the Taconnaz, Mer de Glace, or smaller
323 glaciers such as Pierre Joseph or Aiguille des Glaciers, show steadier values. Most glaciers with strong seasonality show
324 distinct high velocity peaks that appear in summer/late summer (July to October) and minima that normally occur during mid-



325 winter (January to April). Some of the series show stronger interannual variations and this is particularly noticeable on Brenva
 326 Glacier and Charpoua Glacier.



327
 328 **Figure 7. Time series of monthly glacier surface velocities over the 2016-2022 period. Robust linear trends calculated on each full**
 329 **period (i.e.: 2016-2019 and 2020-2022) are highlighted in solid red (t -statistics > 2) and dashed black (t -statistics < 2) lines. Coloured**
 330 **markers refer to the glacier classification.**

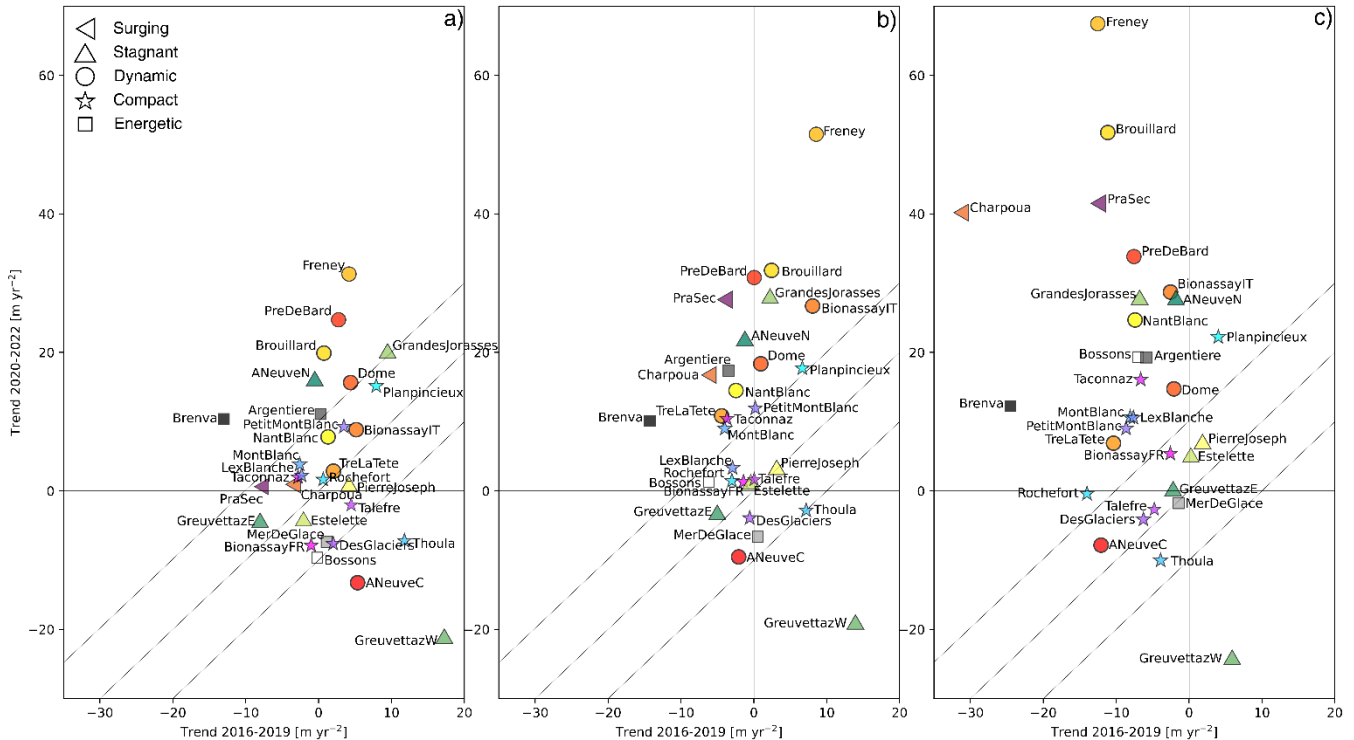
331 Pra Sec and Charpoua, in particular, show very low minimum velocities (in the range of 25 m yr^{-1} to 50 m yr^{-1}) but very high
 332 peaks with a max/min ratio that can reach a 7:1 value. These velocity peaks seem to appear in summer/late summer and extreme
 333 velocity changes from winter to summer velocities can be noticed (Pra Sec 2022, Charpoua 2018). Charpoua Glacier shows



334 seasons with high summer peaks (2016, 2018) and other summer seasons that maintain particularly low displacements
335 throughout the entire summer (2017, 2019, 2021). Pra Sec Glacier seems to display more regular annual summer speed ups:
336 in the period analysed, every summer had a strong velocity peak only, except 2018.

337 The analysis of the time series shows that many glaciers had a positive trend of velocity starting from 2020, which is
338 particularly evident in some glaciers like Argentière, Biossanay (IT), Brouillard, Freney, Pré de Bard. To statistically and
339 quantitatively estimate this behaviour, we divided the full timespan into two periods: a first period between 2016 and 2019,
340 and a second one between 2020 and 2022 (Figure 7). Subsequently, we applied a robust linear regression to each full period
341 (i.e., considering all the monthly data) and only to winter (i.e., from December to April) and summer (i.e., from July to
342 September) months. Figure 8 shows the linear trends of the first vs second period in the three cases. Considering the winter
343 months, a well-defined general behaviour is not clearly noticeable. In the first period, most velocity trends are included in the
344 range $\pm 10 \text{ m yr}^{-2}$, 11 have negative trends and 19 positives; the trends in the second period are in general similar to those of
345 the first, with exception of six glaciers that show an increase compared to the first period (i.e., Trend in 2019–2022 minus
346 Trend in 2016–2019, t_2-t_1), of $t_2-t_1 > 10 \text{ m yr}^{-2}$, and three with a decrease $t_2-t_1 < 10 \text{ m yr}^{-2}$ (Figure 8a). Considering the full year,
347 in the first period, the velocity trends are basically the same as those of the winter case; while in the second period, 17 glaciers
348 showed a velocity increase of $> 10 \text{ m yr}^{-2}$ and seven glaciers an increase of $> 20 \text{ m yr}^{-2}$. Overall, 24 glaciers showed an
349 acceleration (or a decrease of deceleration, i.e., $t_2-t_1 > 0$) between the first and second periods, of which 17 glacier $t_2-t_1 > 10 \text{ m}$
350 yr^{-2} and 9 glacier $t_2-t_1 > 20 \text{ m yr}^{-2}$ (Figure 8b). Considering the summer months, in the first period, most glaciers (26 of 30) have
351 negative velocity trends, while in the second period, 23 glaciers show positive acceleration of which 17 glaciers have trends
352 $> 10 \text{ m yr}^{-2}$ and 12 glaciers $> 20 \text{ m yr}^{-2}$. Overall, 27 glaciers have a velocity trend in the second period greater than in the first
353 period, in 20 glaciers, the difference between second and first period is at least $t_2-t_1 > 10 \text{ m yr}^{-2}$, and in 13 cases the difference
354 is $t_2-t_1 > 20 \text{ m yr}^{-2}$ (Figure 8c). Overall, we observed that the trends included in the range $\pm 10 \text{ m yr}^{-2}$ had t -statistics (i.e., linear
355 slope divided by its standard error) < 2 , thus they were less statistically significative.

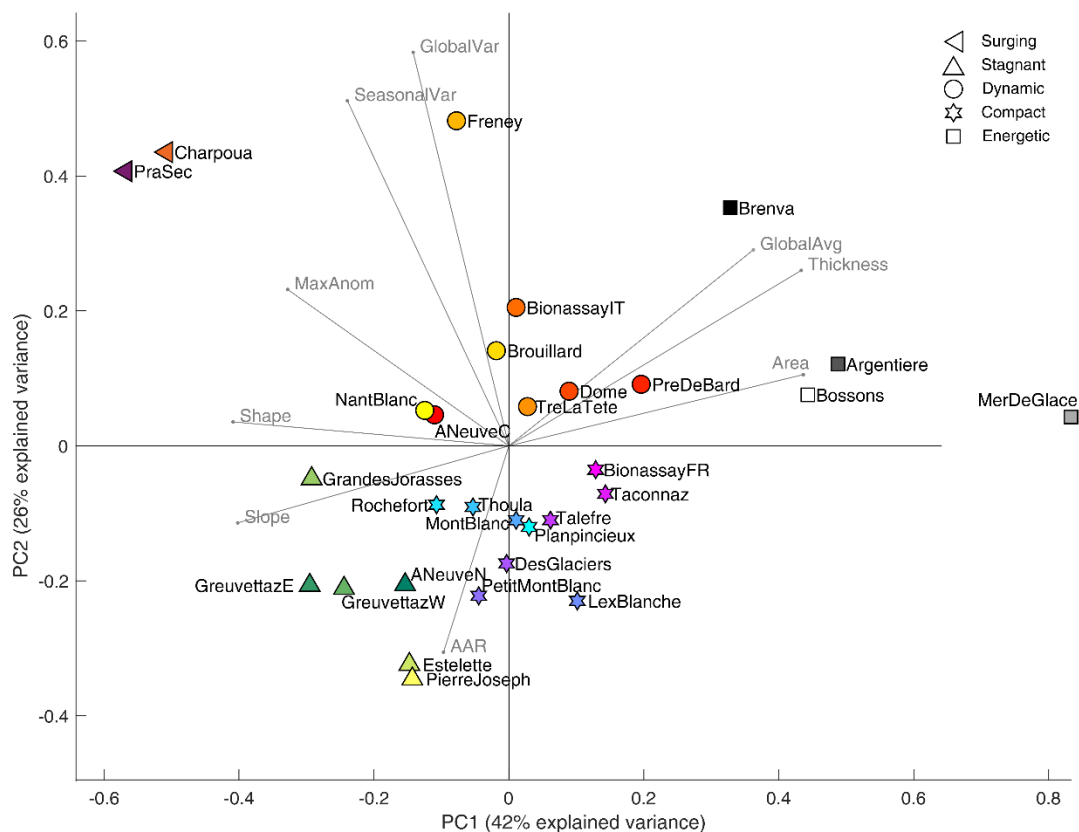
356



357
 358 **Figure 8.** Annual velocity variations of the glaciers during the period 2016-2019 (x-axis) and 2020-2022 (y-axis). Trends have been
 359 calculated using: in a) cold months (from November to April); in b) every month (i.e., From January to December), while in c) warm
 360 months (from June to September). The oblique lines indicate the boundary where the difference between the trends of the two
 361 periods (second minus first period) is $+10 \text{ m yr}^{-2}$, 0 m yr^{-2} and -10 m yr^{-2} , respectively from the upper to the lower line. Markers
 362 indicate the glacier class.

363 5.6 Glacier classification

364 The investigation of the possible presence of distinct classes of glacier based on their morphodynamics using PCA and K-
 365 means clustering is hereby presented. Figure 9 shows the biplot of the two principal components (PCs). The first PC (PC1)
 366 accounts for 42% of the explained variance of the dataset. It is principally composed of the morphological features - Area and
 367 Thickness contribute positively; Shape and Slope negatively - and glacier flow velocity (GlobalAvg). Accordingly, wide,
 368 compact (i.e., non-elongated), gentle and fast glaciers have PC1 high positive values. On the other hand, PC2 explains 26% of
 369 the dataset variance and is mainly formed of kinematic features and AAR, which contributes negatively. In this case, glaciers
 370 with high velocity variability and small accumulation areas assume PC2 high positive values. Based on the two first PCs, an
 371 unsupervised K-mean clustering identified five classes of glacier.



372
 373 **Figure 9. Biplot of the two principal components describing the variance of the dataset. Five clusters of glaciers are identified and**
 374 **highlighted by different markers.**

375 6 Discussion

376 6.1 Velocity trends and comparison with other regional studies

377 Concerning the time series analysis, we compared our observations with similar existing studies in this region considering two
 378 long-term glacier velocity records in the Argentière Glacier (Vincent and Moreau, 2016) and Miage Glacier (Smiraglia et al.,
 379 2000; Fyffe, 2012). At Argentière Glacier, a unique series of continuous basal sliding measurements exist from 1997 and was
 380 still active as of 2022 (Vincent et al., 2022; Nanni et al., 2020). The whole series indicates a general decrease in basal sliding
 381 velocities (Vincent and Moreau, 2016) since the end of the 1990s. This general decrease has shown a strong correlation with
 382 the negative mass balance of the glacier, which agrees with the conceptual model from Span and Kuhn (Span and Kuhn, 2003),
 383 in which the glacier flow variation is primarily driven by the mass balance of the accumulation area in the previous year (as it
 384 determines glacier thickness variations). Seasonal field surveys conducted at Argentière Glacier from the 1950s document a
 385 longer data series than the basal sliding measurements started in 1997, and an increase of surface velocities was clearly
 386 measured during a period of positive mass balances in the early 1980s (Vincent and Moreau, 2016). The same trend was
 387 highlighted by Span and Kuhn (Span and Kuhn, 2003) for at least six other glaciers: Saint Sorlin in France, Gietro and
 388 Corbassiere in Switzerland, and Pasterze, Vernagtferner and Odenwinkelkees in Austria. At Miage Glacier, surface velocities



389 have been measured historically by different authors (Diolaiuti et al., 2005; Smiraglia et al., 2000; Fyffe, 2012; Lesca, 1974;
390 Pelfini et al., 2007; Deline, 2002) and also show a general velocity decrease in recent decades. (Smiraglia et al., 2000; Fyffe,
391 2012). Globally, glacier slowdown linked to negative mass balance trend was also shown for six different regions around the
392 globe and dates spanning from 1953 to 2009 by Heid and Kaab in 2012 (Heid and Käab, 2012a) by an analysis of remotely-
393 sensed optical images. Specific analysis of velocity trends and glacier mass loss showed generalized decreasing velocity trends
394 over different regions of High Mountain Asia between 2000 and 2017 and a strong correlation with the negative mass balance
395 trend (Dehecq et al., 2019).

396 According to the observations at the Argentière and Miage glaciers, the signal of velocity decrease from the early 2000s can
397 be linked to continuous negative mass balances (Vincent and Moreau, 2016) of most Alpine glacier since the 2000s (Zemp et
398 al., 2021). The results of our study agree with this negative trend in the first part of the considered period (i.e., 2016–2019),
399 but we detected an inverse trend and a velocity rise from 2020 occurring in most glaciers under study. Notably, the velocity
400 trend inversion in the recent years is most visible during the warm season, while there is not a clear signal in winter. An
401 accelerating trend ($+5 \text{ m yr}^{-2}$ between 2015–2021) has recently been shown for the Brenva Glacier by an analysis of remotely-
402 sensed optical images (Rabatel et al., 2023). Besides, (Rabatel et al., 2023) observed a slight ice thickening ($\sim 1 \text{ m}$ between
403 2000 and 2019) in an upper sector of the Brenva Glacier. They proposed three hypotheses to explain the acceleration of the
404 Brenva: a) a glacier thickening; b) a change in thermal regime; and c) a change in subglacial hydrology, possibly related to an
405 increased ablation in the upper reaches of the glacier (Rabatel et al., 2023). Even though the hypothesis of glacier thickening
406 could explain the specific case of Brenva, the glacier surface elevation change across the Mont Blanc massif has been generally
407 negative in the last years, as evidenced by the negative mass balance of the reference glaciers in the area (Zemp et al., 2021;
408 Zemp et al., 2009). Local anomalies of positive mass balance could explain an increase of velocity but the lack of measurements
409 at higher altitudes does not allow us to confirm this behaviour at present. However, the meteorological conditions in the recent
410 years have remained approximately constant, with slight trends of increasing temperature and decreasing precipitation between
411 2020–2022 that make unlikely a general glacier thickening in the region (Figure S3). Localized high rates of accumulation due
412 to increased avalanche activity and wind accumulation should also contribute to the ice thickening (thus yielding an
413 acceleration), but cannot be investigated at this stage. In any case, these hypotheses can be valid for specific sectors of glaciers,
414 while we observed a generalised acceleration across the region; thus, glacier thickening seems not to be the most relevant
415 forcing of velocity increase. A variation of the hydrology of groups of glaciers could be more reasonable, especially if they lie
416 in neighbouring basins, but is unlikely to occur contemporary over the whole region. On the other hand, the distribution of the
417 acceleration trend over different areas of the massif and regarding different classes of glaciers suggest the existence of a
418 climatic driver of the phenomenon. Therefore, a thermal regime change could explain the velocity rise. The fact that the
419 acceleration is most evident during the warm season seems to corroborate this hypothesis, even though the mean summer
420 temperature was slightly lower (-0.2°C) in 2020–2022 than in 2016–2019 (Table S1). In the end, a definitive answer cannot be
421 formulated so far and further research is necessary to understand the processes involved in this trend.

422 The general acceleration detected in the study should be monitored in the future. In fact, if this trend continues, it should be
423 also considered that an acceleration trend over few years (2012–2016) has been measured before the large destabilization of
424 Aru 1 Glacier (Gilbert, 2018). However, the trend highlighted in our study is detected over a short period (2020–2022) and
425 could be a fluctuation onset on a generally decreasing trend at a decadal scale. In any case, the causes of such an anomaly
426 should be a matter of further research.

427 **6.2 Glacier classification**

428 In regard to glacier classification, we individuated five groups:



429 ‘*Surging glaciers*’: only two glaciers belong to this group: Charpoua and Pra Sec. They are thin small steep elongated glaciers.
430 Their average velocity is rather low but they feature a much stronger annual cycle with periods of surge-like dynamics during
431 which they occasionally show accelerations of almost one order of magnitude. Possible glacier advances are prevented by the
432 steep bedrock cliff at the snout, which causes the disintegration of the glacier by repeated ice falls from the glacier front
433 (Giordan et al., 2020; Pralong and Funk, 2006). Both glaciers have had documented ice avalanche activity from their frontal
434 areas (Buisson et al., 1999; Mourey and Ravanel, 2017; Ravanel, 2009; Deline et al., 2010). Ice avalanches from the Pra Sec
435 Glacier occurred in the 1930s, in August 1981 (Deline et al., 2010), and repeatedly in 2020 and 2021 (Forestry Service of
436 Aosta Valley, personal communication). Ice avalanches from the Charpoua snout between 40000 and 60000 m³ occurred in
437 1997 (Deline et al., 2010; Deline et al., 2012) and 2018 (Lehmann, 2018 - <https://news.unil.ch/display/1536777918113>,
438 accessed online 11 October 2023). During 2018, a strong summer acceleration was highlighted in the present study at Charpoua
439 Glacier. The precursory acceleration before a failure has been investigated and measured in landslides and rockfalls (Fukuzono,
440 1985), cold-based glaciers (Faillettaz et al., 2016) and, in a few cases, temperate or polythermal glaciers (Giordan et al., 2020;
441 Faillettaz et al., 2012).

442 Elevation changes typical of surging glaciers should be investigated to better describe such processes but, presently, such data
443 is not available. As far as we know, to date, such surge-like behaviour on small steep temperate Alpine glaciers have not been
444 documented.

445 ‘*Stagnant glaciers*’: they are morphologically similar to *surging glaciers* (i.e., small, steep and elongated). *Stagnant glaciers*
446 lie, in general, at high altitudes, thus they have a larger AAR compared to other glaciers (in particular *surging glaciers*). The
447 velocity seasonal cycle is modest or even non-detectable since the velocity in winter is close to the measurement uncertainty
448 (besides the Grandes Jorasses, which has a relatively pronounced seasonal cycle). It is worth highlighting that signals of
449 potential velocity fluctuations could exist but remotely-sensed data are not currently suited for the analysis of such small
450 glaciers.

451 ‘*Dynamic glaciers*’: the morphology of these glaciers is less homogeneous, even though most are generally gentler and thicker
452 than average. They all feature strong kinematic activity, their velocity is higher than average with marked variability and they
453 often show a pronounced regular annual cycle, as in the case of the Bionassay (IT) and Freney glaciers. A large ice avalanche
454 event was documented in 1956 at Freney Glacier (Chiarle et al., 2023), which is one of the glaciers displaying some of the
455 largest velocity variations in this group. A possible correlation between summer accelerations and glacier destabilisations that
456 can lead to ice avalanche processes would need further research; in any case, this would be more site-specific research and
457 goes beyond the scope of the present study.

458 ‘*Compact glaciers*’: gentle, medium-sized glaciers that are not very elongated. Morphologically similar to *dynamic glaciers*
459 but generally thinner, they are markedly less active. In particular, even though some display a regular seasonal cycle (e.g.,
460 Planpincieux, Mont Blanc, Rochefort), their velocity variability and average thickness are much lower, comparable to the
461 *stagnant glaciers*. Since their extension is limited, the areas suitable for the analysis presented in this study can also be small
462 and influence the quality of the output. This group of glaciers would probably be better analysed using higher resolution
463 imagery and higher frequency image acquisition.

464 ‘*Energetic glaciers*’: this group includes large and thick glaciers which are not very elongated. *Energetic glaciers* have
465 accumulation areas located at high altitudes; they show high surface velocities across the whole year and seldom display
466 seasonal variations (except Brenva, which follows an evident seasonal cycle). Their morphology is complex - e.g., the slope
467 varies considerably. In the present study, we concentrated the analyses on the middle sectors of the glaciers where the quality
468 of the velocity data was higher. Since they are large, reach a low altitude and have flat and little crevassed valley tongues, they
469 have often been historically chosen for glaciological field surveys (Span and Kuhn, 2003). Therefore, the knowledge of Alpine



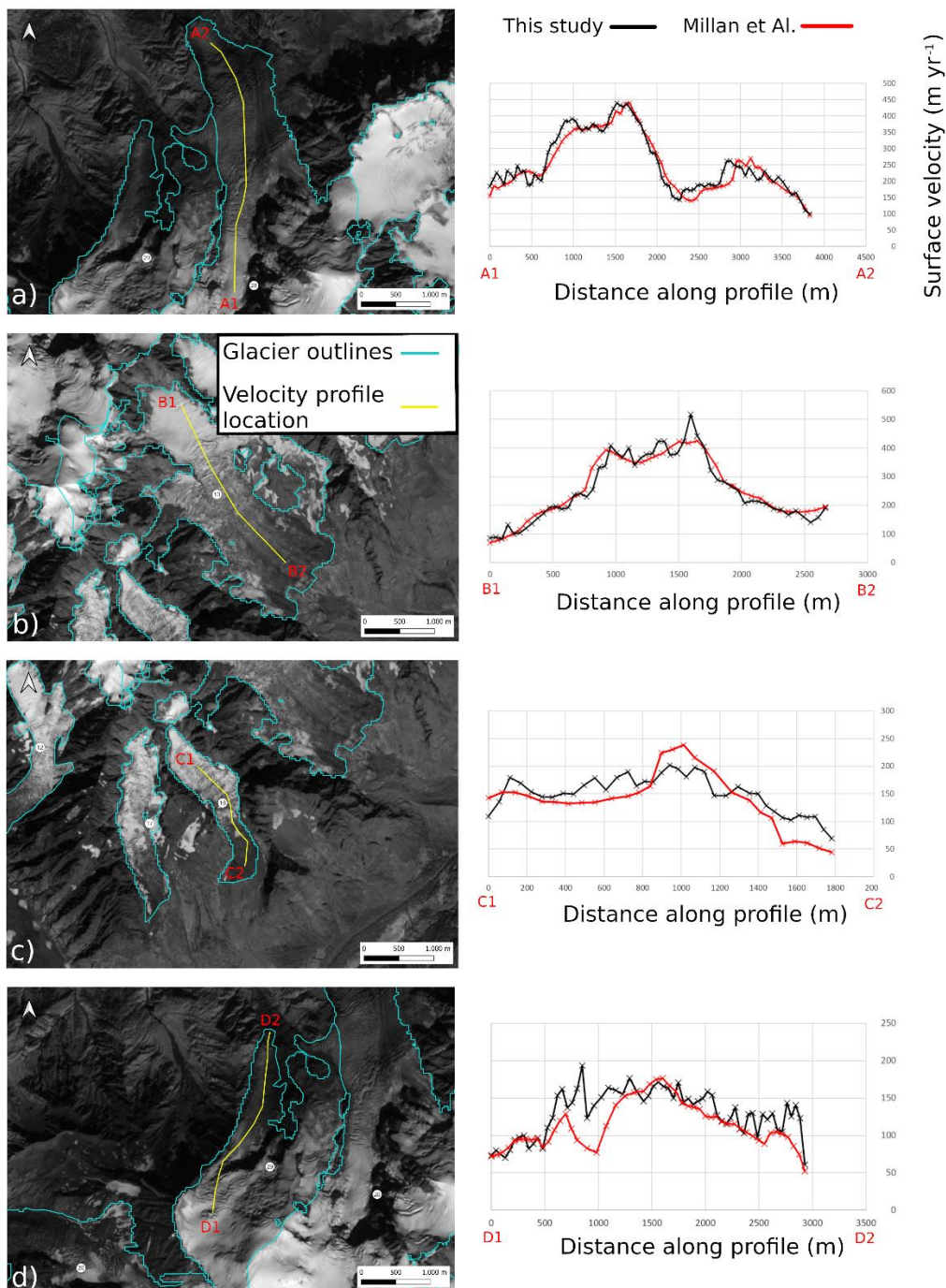
470 glaciers kinematics is generally mostly related to this type of glacier, which can be significantly different compared to the
471 other glacier groups analysed in this study.

472 **6.3 Uncertainty analysis**

473 To estimate the quality of our data, we performed two investigations. First, following the method proposed by (Millan et al.,
474 2019), we calculated the standard deviation of the monthly time series during the whole period 2016–2022 on a set of 155
475 points selected on stable terrain; subsequently, we consider the median of these standard deviations, obtaining an uncertainty
476 of 10.9 m yr^{-1} . In their study, (Millan et al., 2019) estimated the nominal precision according to the temporal baseline between
477 the correlated images, which they found being between $6\text{--}16 \text{ m yr}^{-1}$ for baselines respectively of 40 and 20 days, which is the
478 typical range of temporal gaps between images used in our study. Moreover, the value of 10.9 m yr^{-1} is in close agreement
479 with the uncertainty found by (Mouginot et al., 2023), which obtained a root mean squared error of 10.5 m yr^{-1} between glacier
480 velocities measured over the Mer de Glace and Argètiere glaciers using image correlation of Sentinel2 images and GNSS in
481 situ data (<https://glacioclim.osug.fr/>).

482 Second, we considered the glacier velocity from (Millan et al., 2019), who published mean annual velocity in the period 2017–
483 2018 on a $50 \times 50 \text{ m}$ regular grid. They adopted normalised cross-correlation and chip size refinement (initial size of $16 \times 16 \text{ px}$).
484 They estimated an overall uncertainty of glacier surface velocity time series of $\sim 12 \text{ m yr}^{-1}$ over the Mont Blanc glaciers, and,
485 specifically at Brenva and Bosson glacier, an uncertainty of $15\text{--}20 \text{ m yr}^{-1}$. We compared these data and ours along four glacier
486 longitudinal central lines (i.e., in Bossons, Brenva, Freney and Tacconnaz), obtaining good agreement (Figure 10). The largest
487 differences ($>50 \text{ m yr}^{-1}$) were found in a specific sector of the Tacconnaz Glacier (Figure 10d), where the flux is highly
488 channelized in a narrow passage. There, the data of (Millan et al., 2019) show a velocity decrease that seems unlikely
489 considering the geometry of the site. However, the velocity profiles are similar elsewhere. On average, the surface velocities
490 that we obtained are slightly higher, with difference mean $+6.6 \text{ m yr}^{-1}$ and root mean squared deviation (RMSD) of 28.2 m yr^{-1}
491 (Table 2). The slightly higher RMSD compared to the expected uncertainty can be due to the fact that the precision in
492 glacierized areas is probably larger (less precise) than in ice-free zones because the surface texture is different and changes
493 (e.g., snow precipitation, surface melt, glacier movement) occur more rapidly, therefore causing more decorrelation (Millan et
494 al., 2019).

495



496
 497 **Figure 10. Comparison of velocity profiles from Millan et al. (2022) (red) and from this study (black) at: (a) Bossons Glacier, (b)**
 498 **Brenva Glacier, (c) Freney Glacier and (d) Taconnaz Glacier. Higher altitude to the left, lower altitude to the right, traced along**
 499 **profiles in yellow on the corresponding maps. Sentinel-2 image base map (B08 band), courtesy of the Copernicus Open Access Hub**
 500 **(<https://scihub.copernicus.eu>, last access: 10 September 2023).**



501 **Table 2. Mean difference and root mean squared deviation (RMSD) between this study and Millan et al. (2022) along velocity**
502 **longitudinal profiles.**

	Bossons	Brenva	Freney	Taconnaz	Mean all profiles	
503						
504						
505	Mean [m yr ⁻¹]	3.2	5.9	6.7	10.7	6.6
506	RMSD [m yr ⁻¹]	28.9	33.3	30.2	20.6	28.2
507						

508 **6.4 Limits of the proposed methodology**

509 The methodology presented in this study allow the detection of anomalous accelerations of glaciers, which can be precursors
510 of ice avalanches (Pralong et al., 2005; Failletaz et al., 2008; Giordan et al., 2020). In this frame, it would be very relevant to
511 measure and know typical velocity fluctuations of specific glaciers in stable conditions. This could allow an assessment and
512 to what extent a suspect acceleration may be anomalous and potentially destabilising, bearing in mind that high-rate monitoring
513 is essential to detect glacial instabilities, since the expected sharp increase in velocity in the weeks before the failure (Pralong
514 and Funk, 2006) could be hardly detectable from remote sensing (e.g., due to scarce visibility, image decorrelation, low
515 resolution).

516 Limits of the methodology presented in this study should also be considered: considering the estimated precision of ~11 m yr⁻¹
517 and the usual revisiting time between available images (i.e., with sufficient visibility), which typically ranged between 20 to
518 40 days, the minimum measurable velocity is approximatively 40 m yr⁻¹. Glacier moving at slower rates can be surveyed using
519 larger temporal baselines (Millan et al., 2019; Mouginot et al., 2023), but this implies reducing the ability to catch short-term
520 velocity fluctuations, like those observed at Charpoua and Pra Sec glaciers. Another known issue pertains to the lack of features
521 of the glacier surface that makes it impossible to track movements using optical imagery. Satellite optical imagery is limited
522 and can be strongly influenced by the presence of clouds that could yield extensive periods without data acquisition, even
523 though, in the present study, few limiting conditions have occurred (four months with no data out of eighty processed months
524 of available imagery). Anomalies due to image decorrelation for the presence of shadows, snow or morphological surface
525 modifications can occur and an expert-based visual check may be required to discriminate anomalous velocities.

526 **7 Conclusions**

527 In the present study, we produced ice velocity maps and time series of thirty glaciers of the Mont Blanc massif during the
528 period 2016–2022. The existing publicly available automatically processed velocity datasets, normally have coarse velocity
529 maps (i.e., >100 m), which cannot detect correctly the kinematics of most Alpine glaciers, due to their small size. Therefore,
530 specific processing and studies are needed to characterize the surface kinematics of Alpine glaciers. We used Sentinel-2
531 imagery due to its free availability, ground resolution and revisit time in the study area. Using PCA and unsupervised K-means
532 clustering, we proposed a classification of five groups of glaciers based on their morpho-kinematic features. Plus, we observed
533 a significative acceleration trend in most of the studied glaciers in the last years (2020–2022), but the causes are still not well
534 understood.

535 Processing and analysis of such datasets around other massifs in the Alps, and globally, should be a base for stimulating
536 research on high resolution spatiotemporal variations of velocities on Alpine glaciers and, especially, on understanding the
537 variations in the motion of mountain glaciers. A large research question remains open and deals in understanding and



538 measuring the drivers of change in motion of alpine glaciers. This implicates the complex acquisition of data related to the
539 possible drivers of the variations such as mass balances, water inputs and the temporal variations in subglacial hydrology of
540 single glaciers. However, in order to delve further into these investigations, more complete and widespread glacier surface
541 velocity databases such as that presented in this study, are needed to build future research on the topic.

542 **Acknowledgments**

543 The authors would like to thank Jean Pierre Fosson, Raffaele Rocco, Valerio Segor, Guido Giardini for their support and their
544 will to stimulate cryospheric research activities in the Aosta Valley region and on the Italian side of Mont Blanc massif. We
545 thank all the staff at Fondazione Montagna sicura for supporting all the research activities of the research team. Dr Etienne
546 Berthier supplied a processed 2018 Pleiades stereo DEM on which retrieving altitudinal data that was presented in this paper.
547 We thank Prof. Christian Vincent for his advice on research activity and for supplying useful additional information, especially
548 on the French glaciers of Mont Blanc.

549 **Data availability**

550 Glacier outlines shapefiles can be requested by contacting the lead author. Sentinel-2 imagery is available from the Copernicus
551 Open Access Hub (<https://scihub.copernicus.eu>, Copernicus, 2022). The GIV toolbox is freely available online
552 (<https://github.com/MaxVWDV/glacier-image-velocimetry>). The original glacier surface velocity dataset is available for
553 download as a supplement.

554 **Competing interests.** The authors declare that they have no conflict of interest.

555 **Author contributions.** Fabrizio Troilo: Conceptualization, writing – original draft preparation, investigation, methodology,
556 data curation, formal analysis, visualization; Niccolò Dematteis: Writing – review & editing, data curation, methodology,
557 formal analysis, validation, visualization; Francesco Zucca Writing – review & editing, methodology, supervision, validation;
558 Martin Funk Writing – review & editing, supervision; Daniele Giordan: Writing – review & editing, methodology, supervision,
559 validation.

560 **References**

- 561 Ahn, Y. and Box, J. E.: Glacier velocities from time-lapse photos: technique development and first results from the Extreme
562 Ice Survey (EIS) in Greenland, *Journal of Glaciology*, 56, 723-734, 2010.
- 563 Allstadt, K., Shean, D., Campbell, A., Fahnestock, M., and Malone, S.: Observations of seasonal and diurnal glacier velocities
564 at Mount Rainier, Washington, using terrestrial radar interferometry, *The Cryosphere*, 9, 2219-2235, 2015.
- 565 Altena, B., Scambos, T., Fahnestock, M., and Kääb, A.: Extracting recent short-term glacier velocity evolution over southern
566 Alaska and the Yukon from a large collection of Landsat data, *The Cryosphere*, 13, 795-814, 2019.
- 567 Arendt, A., Bliss, A., Bolch, T., Cogley, J., Gardner, A., Hagen, J.-O., Hock, R., Huss, M., Kaser, G., and Kienholz, C.:
568 Randolph Glacier inventory—A dataset of Global glacier outlines: Version 6.0: Technical report, Global land ice measurements
569 from space, 2017.
- 570 Beniston, M., Farinotti, D., Stoffel, M., Andreassen, L. M., Coppola, E., Eckert, N., Fantini, A., Giacona, F., Hauck, C., and
571 Huss, M.: The European mountain cryosphere: a review of its current state, trends, and future challenges, *The Cryosphere*, 12,
572 759-794, 2018.
- 573 Benn, D. I. and Evans, D. J.: *Glaciers & glaciation*, Routledge 2014.



- 574 Beraud, L., Cusicanqui, D., Rabatel, A., Brun, F., Vincent, C., and Six, D.: Glacier-wide seasonal and annual geodetic mass
575 balances from Pléiades stereo images: application to the Glacier d'Argentière, French Alps, *Journal of Glaciology*, 69, 525-
576 537, 2023.
- 577 Berthier, E., Vadon, H., Baratoux, D., Arnaud, Y., Vincent, C., Feigl, K., Remy, F., and Legresy, B.: Surface motion of mountain
578 glaciers derived from satellite optical imagery, *Remote Sensing of Environment*, 95, 14-28, 2005.
- 579 Berthier, E., Vincent, C., Magnússon, E., Gunnlaugsson, Á., Pitte, P., Le Meur, E., Masiokas, M., Ruiz, L., Pálsson, F., and
580 Belart, J.: Glacier topography and elevation changes derived from Pléiades sub-meter stereo images, *The Cryosphere*, 8, 2275-
581 2291, 2014.
- 582 Bindschadler, R.: The importance of pressurized subglacial water in separation and sliding at the glacier bed, *Journal of*
583 *Glaciology*, 29, 3-19, 1983.
- 584 Buisson, A., Dumas, C., Reynaud, L., and Valla, F.: Les risques naturels d'origine glaciaire: inventaire dans les Alpes françaises
585 et typologie, *La Houille Blanche*, 47-53, 1999.
- 586 Chiarle, M., Viani C., Mortara G., Deline P., Tamburini A. and Nigrelli G.: Large glacier failures in the Italian Alps over the
587 last 90 years, *Geografia Fisica e Dinamica Quaternaria*, 45, 19-40, 2022.
- 588 Cuffey, K. M. and Paterson, W. S. B.: *The Physics of Glaciers*, Academic Press 2010.
- 589 Dehecq, A., Gourmelen, N., Gardner, A. S., Brun, F., Goldberg, D., Nienow, P. W., Berthier, E., Vincent, C., Wagnon, P., and
590 Trouvé, E.: Twenty-first century glacier slowdown driven by mass loss in High Mountain Asia, *Nature Geoscience*, 12, 22-27,
591 2019.
- 592 Deilami, K. and Hashim, M.: Very high resolution optical satellites for DEM generation: a review, *European Journal of*
593 *Scientific Research*, 49, 542-554, 2011.
- 594 Deline, P.: Étude géomorphologique des interactions entre écroulements rocheux et glaciers dans la haute montagne alpine: le
595 versant sud-est du massif du Mont-Blanc (Vallée d'Aoste, Italie), Chambéry, 2002.
- 596 Deline, P., Gardent, M., Magnin, F., and Ravel, L.: The morphodynamics of the Mont Blanc massif in a changing cryosphere:
597 a comprehensive review, *Geografiska Annaler: Series A, Physical Geography*, 94, 265-283, 2012.
- 598 Deline, P., Bolon, P., Chiarle, M., Fioraso, G., Fosson, J. P., Gay, M., Gardent, M., Di Cella, U. M., Ott, L., and Pogliotti, P.:
599 GlaRiskAlp, a French-Italian project (2010-2013) on glacial hazards in the Western Alps in relation with the glacier retreat,
600 14th Alpine Glaciological Meeting,
- 601 Dematteis, N. and Giordan, D.: Comparison of digital image correlation methods and the impact of noise in geoscience
602 applications, *Remote Sensing*, 13, 327, 2021.
- 603 Dematteis, N., Giordan, D., Troilo, F., Wrzesniak, A., and Godone, D.: Ten-Year Monitoring of the Grandes Jorasses Glaciers
604 Kinematics. Limits, Potentialities, and Possible Applications of Different Monitoring Systems, *Remote Sensing*, 13, 3005,
605 2021.
- 606 Diolaiuti, G., Kirkbride, M., Smiraglia, C., Benn, D., D'agata, C., and Nicholson, L.: Calving processes and lake evolution at
607 Miage glacier, Mont Blanc, Italian Alps, *Annals of Glaciology*, 40, 207-214, 2005.
- 608 Einarsson, B., Magnússon, E., Roberts, M. J., Pálsson, F., Thorsteinsson, T., and Jóhannesson, T.: A spectrum of jökulhlaup
609 dynamics revealed by GPS measurements of glacier surface motion, *Annals of Glaciology*, 57, 47-61, 2016.
- 610 Evans, A. N.: Glacier surface motion computation from digital image sequences, *IEEE Transactions on Geoscience and Remote*
611 *Sensing*, 38, 1064-1072, 2000.
- 612 Fahnestock, M., Scambos, T., Moon, T., Gardner, A., Haran, T., and Klinger, M.: Rapid large-area mapping of ice flow using
613 Landsat 8, *Remote Sensing of Environment*, 185, 84-94, 2016.
- 614 Faillietaz, J., Funk, M., and Sornette, D.: Instabilities on Alpine temperate glaciers: new insights arising from the numerical
615 modelling of Allalingsletscher (Valais, Switzerland), *Natural Hazards and Earth System Sciences*, 12, 2977-2991, 2012.
- 616 Faillietaz, J., Funk, M., and Vagliasindi, M.: Time forecast of a break-off event from a hanging glacier, *The Cryosphere*, 10,
617 1191-1200, 2016.
- 618 Faillietaz, J., Pralong, A., Funk, M., and Deichmann, N.: Evidence of log-periodic oscillations and increasing icequake activity
619 during the breaking-off of large ice masses, *Journal of Glaciology*, 54, 725-737, 2008.
- 620 FUKUZONO, T.: A method to predict the time of slope failure caused by rainfall using the inverse number of velocity of
621 surface displacement, *Landslides*, 22, 8-13_11, 1985.
- 622 Fyffe, C. L.: *The hydrology of debris-covered glaciers*, University of Dundee, 2012.



- 623 Giordan, D., Dematteis, N., Allasia, P., and Motta, E.: Classification and kinematics of the Planpincieux Glacier break-offs
624 using photographic time-lapse analysis, *Journal of Glaciology*, 66, 188-202, 2020.
- 625 Glen, J.: Experiments on the deformation of ice, *Journal of Glaciology*, 2, 111-114, 1952.
- 626 Gottardi, F., Obled, C., Gailhard, J., and Paquet, E.: Statistical reanalysis of precipitation fields based on ground network data
627 and weather patterns: Application over French mountains, *Journal of hydrology*, 432, 154-167, 2012.
- 628 Heid, T. and Kääb, A.: Repeat optical satellite images reveal widespread and long term decrease in land-terminating glacier
629 speeds, *The Cryosphere*, 6, 467-478, 2012a.
- 630 Heid, T. and Kääb, A.: Evaluation of existing image matching methods for deriving glacier surface displacements globally
631 from optical satellite imagery, *Remote Sensing of Environment*, 118, 339-355, 2012b.
- 632 Humbert, A., Greve, R., and Hutter, K.: Parameter sensitivity studies for the ice flow of the Ross Ice Shelf, Antarctica, *Journal*
633 *of Geophysical Research: Earth Surface*, 110, 2005.
- 634 Jiskoot, H.: Dynamics of Glaciers, *physical Research*, 92, 9083-9100, 2011.
- 635 Jolliffe, I. T. and Cadima, J.: Principal component analysis: a review and recent developments, *Philosophical transactions of*
636 *the royal society A: Mathematical, Physical and Engineering Sciences*, 374, 20150202, 2016.
- 637 Kääb, A., Winsvold, S., Altena, B., Nuth, C., Nagler, T., and Wuite, J.: Glacier Remote Sensing Using Sentinel-2. Part I:
638 Radiometric and Geometric Performance, and Application to Ice Velocity, *Remote Sensing*, 8, 2016.
- 639 Kääb, A., Jacquemart, M., Gilbert, A., Leinss, S., Girod, L., Huggel, C., Falaschi, D., Ugalde, F., Petrakov, D., and
640 Chernomorets, S.: Sudden large-volume detachments of low-angle mountain glaciers—more frequent than thought?, *The*
641 *Cryosphere*, 15, 1751-1785, 2021.
- 642 Kamb, B.: Glacier surge mechanism based on linked cavity configuration of the basal water conduit system, *Journal of*
643 *Geophysical Research: Solid Earth*, 92, 9083-9100, 1987.
- 644 Lesca, C.: Emploi de la photogrammetrie analytique pour la determination de la vitesse superficielle des glaciers et des
645 profondeurs relatives, 1974.
- 646 Luzi, G., Pieraccini, M., Mecatti, D., Noferini, L., Macaluso, G., Tamburini, A., and Atzeni, C.: Monitoring of an alpine glacier
647 by means of ground-based SAR interferometry, *IEEE Geoscience and Remote Sensing Letters*, 4, 495-499, 2007.
- 648 Marsy, G., Vernier, F., Trouvé, E., Bodin, X., Castaings, W., Walpersdorf, A., Malet, E., and Girard, B.: Temporal Consolidation
649 Strategy for Ground-Based Image Displacement Time Series: Application to Glacier Monitoring, *IEEE Journal of Selected*
650 *Topics in Applied Earth Observations and Remote Sensing*, 14, 10069-10078, 2021.
- 651 Millan, R., Mougnot, J., Rabatel, A., and Morlighem, M.: Ice velocity and thickness of the world's glaciers, *Nature*
652 *Geoscience*, 15, 124-129, 2022.
- 653 Millan, R., Mougnot, J., Rabatel, A., Jeong, S., Cusicanqui, D., Derkacheva, A., and Chekki, M.: Mapping surface flow
654 velocity of glaciers at regional scale using a multiple sensors approach, *Remote Sensing*, 11, 2498, 2019.
- 655 Mondardini, L., Perret, P., Frasca, M., Gottardelli, S., and Troilo, F.: Local variability of small Alpine glaciers: Thoula Glacier
656 geodetic mass balance reconstruction (1991-2020) and analysis of volumetric variations, *Geografia Fisica e Dinamica*
657 *Quaternaria*, 44, 29-38, 2021.
- 658 Mougnot, J., Rabatel, A., Ducasse, E., and Millan, R.: Optimization of Cross Correlation Algorithm for Annual Mapping of
659 Alpine Glacier Flow Velocities; Application to Sentinel-2, *IEEE Transactions on Geoscience and Remote Sensing*, 61, 1-12,
660 2023.
- 661 Mourey, J. and Ravel, L.: Evolution of access routes to high mountain refuges of the Mer de Glace Basin (Mont Blanc
662 Massif, France). An example of adapting to climate change effects in the Alpine High mountains, *Journal of Alpine Research*
663 *Revue de géographie alpine*, 2017.
- 664 Nanni, U., Gimbert, F., Vincent, C., Gräff, D., Walter, F., Piard, L., and Moreau, L.: Quantification of seasonal and diurnal
665 dynamics of subglacial channels using seismic observations on an Alpine glacier, *The Cryosphere*, 14, 1475-1496, 2020.
- 666 Nye, J. F.: The mechanics of glacier flow, *Journal of Glaciology*, 2, 82-93, 1952.
- 667 Paradis, E.: Probabilistic unsupervised classification for large-scale analysis of spectral imaging data, *International Journal of*
668 *Applied Earth Observation and Geoinformation*, 107, 102675, 2022.
- 669 Paul, F., Winsvold, S. H., Kääb, A., Nagler, T., and Schwaizer, G.: Glacier remote sensing using Sentinel-2. Part II: Mapping
670 glacier extents and surface facies, and comparison to Landsat 8, *Remote Sensing*, 8, 575, 2016.
- 671 Paul, F., Piermattei, L., Treichler, D., Gilbert, L., Girod, L., Kääb, A., Libert, L., Nagler, T., Strozzi, T., and Wuite, J.: Three
672 different glacier surges at a spot: what satellites observe and what not, *The Cryosphere*, 16, 2505-2526, 2022.



- 673 Paul, F., Rastner, P., Azzoni, R., Diolaiuti, G., Fugazza, D., Le Bris, R., Nemec, J., Rabatel, A., Ramusovic, M., and Schwaizer,
674 G.: Glacier shrinkage in the Alps continues unabated as revealed by a new glacier inventory from Sentinel-2, *Earth Syst. Sci.*
675 *Data*, 12, 1805–1821, 2020.
- 676 Pelfini, M., Santilli, M., Leonelli, G., and Bozzoni, M.: Investigating surface movements of debris-covered Miage glacier,
677 Western Italian Alps, using dendroglaciological analysis, *Journal of Glaciology*, 53, 141–152, 2007.
- 678 Pfeffer, W. T., Arendt, A. A., Bliss, A., Bolch, T., Cogley, J. G., Gardner, A. S., Hagen, J.-O., Hock, R., Kaser, G., and Kienholz,
679 C.: The Randolph Glacier Inventory: a globally complete inventory of glaciers, *Journal of glaciology*, 60, 537–552, 2014.
- 680 Pralong, A. and Funk, M.: On the instability of avalanching glaciers, *Journal of Glaciology*, 52, 31–48, 2006.
- 681 Pralong, A., Birrer, C., Stahel, W. A., and Funk, M.: On the predictability of ice avalanches, *Nonlinear Processes in Geophysics*,
682 12, 849–861, 2005.
- 683 Rabatel, A., Ducasse, E., Ramseyer, V., and Millan, R.: State and Fate of Glaciers in the Val Veny (Mont-Blanc Range, Italy):
684 Contribution of Optical Satellite Products, *Journal of Alpine Research | Revue de géographie alpine*, 2023.
- 685 Rankl, M., Kienholz, C., and Braun, M.: Glacier changes in the Karakoram region mapped by multimission satellite imagery,
686 *The Cryosphere*, 8, 977–989, 2014.
- 687 Ravel, L.: Évolution géomorphologique de la haute montagne alpine dans le contexte actuel de réchauffement climatique,
688 2009.
- 689 Samsonov, S., Tiampo, K., and Cassotto, R.: SAR-derived flow velocity and its link to glacier surface elevation change and
690 mass balance, *Remote Sensing of Environment*, 258, 112343, 2021.
- 691 Scambos, T. A., Dutkiewicz, M. J., Wilson, J. C., and Bindshadler, R. A.: Application of image cross-correlation to the
692 measurement of glacier velocity using satellite image data, *Remote sensing of environment*, 42, 177–186, 1992.
- 693 Schwalbe, E. and Maas, H.-G.: The determination of high-resolution spatio-temporal glacier motion fields from time-lapse
694 sequences, *Earth Surface Dynamics*, 5, 861–879, 2017.
- 695 Smiraglia, C., Diolaiuti, G., Casati, D., and Kirkbride, M. P.: Recent areal and altimetric variations of Miage Glacier (Monte
696 Bianco massif, Italian Alps), IAHS-AISH publication, 227–233, 2000.
- 697 Span, N. and Kuhn, M.: Simulating annual glacier flow with a linear reservoir model, *Journal of Geophysical Research:*
698 *Atmospheres*, 108, 2003.
- 699 Stocker-Waldhuber, M., Fischer, A., Helfricht, K., and Kuhn, M.: Long-term records of glacier surface velocities in the Ötztal
700 Alps (Austria), *Earth system science data*, 11, 705–715, 2019.
- 701 Van Wyk De Vries, M. and Wickert, A. D.: Glacier Image Velocimetry: an open-source toolbox for easy and rapid calculation
702 of high-resolution glacier velocity fields, *The Cryosphere*, 15, 2115–2132, 10.5194/tc-15-2115-2021, 2021.
- 703 Vincent, C. and Moreau, L.: Sliding velocity fluctuations and subglacial hydrology over the last two decades on Argentière
704 glacier, Mont Blanc area, *Journal of Glaciology*, 62, 805–815, 2016.
- 705 Vincent, C., Gilbert, A., Walpersdorf, A., Gimbert, F., Gagliardini, O., Jourdain, B., Roldan Blasco, J. P., Laarman, O., Piard,
706 L., and Six, D.: Evidence of seasonal uplift in the Argentière glacier (Mont Blanc area, France), *Journal of Geophysical*
707 *Research: Earth Surface*, 127, e2021JF006454, 2022.
- 708 Willis, I. C.: Intra-annual variations in glacier motion: a review, *Progress in Physical Geography*, 19, 61–106, 1995.
- 709 Zekollari, H., Huss, M., and Farinotti, D.: Modelling the future evolution of glaciers in the European Alps under the EURO-
710 CORDEX RCM ensemble, *The Cryosphere*, 13, 1125–1146, 2019.
- 711 Zemp, M., Hoelzle, M., and Haeberli, W.: Six decades of glacier mass-balance observations: a review of the worldwide
712 monitoring network, *Annals of Glaciology*, 50, 101–111, 2009.
- 713 Zemp, M., Nussbaumer, S. U., Gärtner-Roer, I., Bannwart, J., Paul, F., and Hoelzle, M.: Global Glacier Change Bulletin Nr. 4
714 (2018–2019), *WGMS*, 4, 2021.
- 715 Zemp, M., Huss, M., Eckert, N., Thibert, E., Paul, F., Nussbaumer, S. U., and Gärtner-Roer, I.: Brief communication: Ad hoc
716 estimation of glacier contributions to sea-level rise from the latest glaciological observations, *The Cryosphere*, 14, 1043–1050,
717 2020.

718

719